Remote Sensing of Environment 181 (2016) 122–136

Contents lists available at ScienceDirect

Remote Sensing of Environment

journal homepage: www.elsevier.com/locate/rse

Global-scale surface roughness effects at L-band as estimated from SMOS observations

Marie Parrens [a,*], Jean-Pierre Wigneron [b], Philippe Richaume [a], Arnaud Mialon [a], Ahmad Al Bitar [a], Roberto Fernandez-Moran [b], Amen Al-Yaari [b], Yann H. Kerr [a]

[a] Centre dEtudes Spatiales de la BIOsphre (CESBIO), UMR5126, BPI 2801, 31401 Toulouse Cedex 9, France
[b] INRA, UR1263 ISPA, F-33140 Villenave d'Ornon, Centre INRA Bordeaux, Aquitaine, France

ARTICLE INFO

Article history:
Received 22 December 2015
Received in revised form 23 March 2016
Accepted 8 April 2016
Available online xxxx

Keywords:
Soil moisture
Vegetation optical depth
Soil roughness
L-band
Retrievals
SMOS

ABSTRACT

The Soil Moisture and Ocean Salinity (SMOS) mission is the first satellite dedicated to providing global surface soil moisture products. SMOS operates at L-band (1.4 GHz) and, at this frequency, the signal not only depends on soil moisture and vegetation optical depth but is also significantly affected by surface effects and, in particular, by the soil roughness. However, when dense vegetation is present, the L-band signal is poorly sensitive to the surface effects. First, by using multiple regressions between soil moisture (SM) and brightness temperature (TB) at different incidence angles and polarizations, the SMOS sensitivity to the surface effects was evaluated. A global-scale map of SMOS sensitivity to the surface effects was computed and showed that, for 87% of the land surface, the SMOS observations were sensitive to these effects, while very low sensitivity to the surface effects was estimated over 13% of the land surfaces. For instance, over broadleaf evergreen forest (mainly the Amazon and Congo forests), SMOS was sensitive to the surface effects over only half of the pixels considered. In a second step, in L-MEB (L-band Microwave Emission of the Biosphere), the forward emission model of the SMOS algorithm, the vegetation and roughness effects were combined in a single parameter, referred to as TR in this study. By inverting L-MEB, SM and TR were retrieved at global scale from the SMOS Level 3 (L3) TB observations during 2011. Assuming a linear relationship between TR and the Leaf Area Index (LAI) obtained from MODIS data, the effects of roughness (H_r) and vegetation were decoupled and a global map of soil roughness effects was estimated. It was found that the spatial pattern of the H_r values could be related to the main vegetation types. Higher values of roughness ($H_r = 0.32–0.39$) were obtained for forests (broadleaf evergreen, deciduous and mixed coniferous) while lower values ($H_r = 0.14–0.16$) were obtained for deserts, shrubs and bare soils. Intermediate values ($H_r = 0.20–0.23$) were obtained over grasslands, tundra and cultivated land. Over vegetation biomes composed of forests and wooded grasslands, the H_r values were mainly correlated to the vegetation density ($r \sim 0.55$). For deserts, shrubs and bare soils, the H_r values were mainly correlated to the topography slopes ($r \sim 0.53$). The global maps presented in this study could lead to improved retrievals of soil moisture and vegetation optical depth for present and future microwave remote sensing missions such as SMOS and Soil Moisture Active Passive (SMAP).

1. Introduction

Soil moisture (SM) plays a key role in the interactions between the hydrosphere, the biosphere and the atmosphere, as it controls both evaporation and transpiration from bare soil and areas with vegetation, respectively. For many applications, global or continental scale soil moisture maps are needed. Numerous studies have been conducted or are currently underway to obtain soil moisture estimates from spaceborne microwave instruments (Entekhabi et al., 2010; Kerr et al., 2001; Njoku, Jackson, Lakshmi, Chan, & Nghiem, 2003; Wagner, Lemoine, & Rott, 1999). Microwave remote sensing is able to provide quantitative information about the water content of a shallow, near-surface layer (Schmugge, 1983), particularly in the low-frequency microwave region from 1 to 10 GHz. L-band is the optimal wavelength for sensing soil moisture with spaceborne passive microwave instruments (Kerr et al., 2001). The Soil Moisture and Ocean Salinity (SMOS) satellite is the first L-band satellite specifically dedicated to mapping soil moisture over land with a mission objective of 0.04 m^3 m^{-3} over bare and sparsely vegetated areas (Al-Yaari, Wigneron, Ducharne, Kerr, De Rosnay et al., 2014; Al-Yaari, Wigneron, Ducharne, Kerr, Wagner et al., 2014; Kerr et al., 2001; Kerr, Waldteufel, Wigneron et al., 2010). The temporal resolution of SMOS is three days with a nominal spatial resolution of 43 km. The recent Soil Moisture Active Passive (SMAP) satellite also maps soil moisture at L-band with a spatial resolution of ≈40 km (Entekhabi et al., 2010).

* Corresponding author.
E-mail address: marie.parrens@cesbio.cnes.fr (M. Parrens).

http://dx.doi.org/10.1016/j.rse.2016.04.006
0034-4257/

The passive microwave emissivity of land surfaces is mainly determined by the characteristics of the soil and vegetation, except for regions covered by open water or snow cover. The main soil characteristics affecting the microwave emissivity are soil moisture, surface roughness, and soil structure and texture. The vegetation layer attenuates the emissivity of the soil and emits its own contribution. This layer is characterized by its water content, geometric structure, and spatial distribution of the trunks, branches and leaves. To model all these characteristics in a radiative transfer model, a large number of parameters are required. Very good knowledge of these parameters is required to obtain high quality estimates of soil moisture. Moreover, the passive microwave sensors have coarse spatial resolution (typically around 10–60 km), so there is generally a variety of land uses and cover, and soil and vegetation types in the sensor footprint. Currently, it is not possible to parameterize the soil and vegetation effects for all the land covers in the radiative transfer model. Only a reduced number of these parameters, referred to as effective parameters (Wigneron, Laguerre, & Kerr, 2001), are usually used in the soil moisture retrieval algorithms. The accuracy of the soil moisture retrievals over vegetated land surfaces depends, to a great extent, on the modeling used to represent the effects of vegetation and roughness. The denser the vegetation layer is, the smaller is the influence of the soil layer on the measured signal (Grant et al., 2008; Kirdyashev, Chukhlantsev, & Shutko, 1979). So, soil moisture retrievals will be less accurate over dense forests than over sparse vegetation.

Similarly, the modeling of the soil roughness effects plays a key role in the SM retrieval algorithm at L-band. Increasing surface roughness effects leads to an increase in the measured brightness temperature (TB) and to a decrease of the sensitivity of the L-band observations to soil moisture. For example, Montpetit et al. (2015) showed that the increase in TB due to the effects of surface roughness could be as large as 45 K for wet soils and 25 K for dry soils when very rough soils were compared with smooth surfaces. The decrease in the slope of the relationship between reflectivity and SM was about 33% between a smooth surface ($\sigma = 0.05$ mm) and a rough surface ($\sigma = 30$ mm). In the SMOS algorithm, the effects of soil roughness are computed by using a semi-empirical model (Wegmuller & Matzler, 1999; Wigneron et al., 2011) initially developed by Wang and Choudhury (1981). This model is based on four roughness parameters: Q_r accounts for the polarization mixing effects (dimensionless number), H_r accounts for the roughness intensity (dimensionless number, frequency dependent) and N_{rp} governs the angular dependence of the reflectivity caused by the rough surface (dimensionless number). To investigate the value of these model parameters, a variety of ground measurements and airborne campaigns at L-band and over different types of vegetation have been carried out in the past (Cano et al., 2010; Escorihuela et al., 2007; Grant et al., 2007; Lawrence, Wigneron, Demontoux, Mialon, and Kerr, 2013; Mo, Choudhury, Schmugge, Wang, and Jackson, 1982; Saleh et al., 2007; Schlenz, Fallmann, Marzahn, Loew, and Mauser, 2012; Wang et al., 1982; Wigneron et al., 2001, 2007, 2011, 2012 among others). These studies provide only local estimates of the roughness parameter values and, even for the same types of soil conditions, the values of the parameter may differ. Moreover, the scale of all these previous studies was not representative of the large satellite footprints of spaceborne sensors. In parallel, several airborne campaigns have been carried out with the same aim (Jackson, Schmugge, and O'Neill, 1984; Merlin, Walker, Panciera, Escorihuela, and Jackson, 2009; Panciera, Walker, Kalma, et al., 2009; Panciera, Walker, and Merlin, 2009; Panciera et al., 2014; Peischl et al., 2012; Saleh et al., 2004, 2009 among others). Despite a larger spatial resolution, the roughness parameter values were difficult to estimate and no consensus emerged.

As it is usually difficult to decouple the effects of surface roughness and vegetation on the passive microwave signal, some SM retrieval algorithms propose to combine the vegetation and roughness effects in a single parameter (referred to as TR in this study) so as to reduce the number of unknown parameters. In this paper, the TR parameter is defined as $TR = H_r/2 + \tau_{nad}$, where H_r is the soil roughness parameter and τ_{nad} is the vegetation optical depth. For example, this is the case for the NASA Advanced Microwave Scanning Radiometer (AMSR-E) algorithm (Njoku & Chan, 2006), the AMSR-E Land Parameter Retrievals Model (Owe, de Jeu, & Walker, 2001) and also for the TRMM TMI SM retrieval algorithm (Bindlish et al., 2003). At L-band, this approach has already been evaluated at local scale by Saleh, Wigneron, de Rosnay, Calvet, and Kerr (2006) and Fernandez-Moran et al. (2015) and at continental USA scale by Parrens, Wigneron et al. (2014).

The aim of this study was to evaluate and map the sensitivity of the L-band microwave observations to soil roughness effects, by analyzing the observations made by SMOS in 2011 at global scale. First, we attempted to classify the land surfaces into two main categories: (1) surfaces where the sensitivity of the SMOS TB observations to the surface effects is very low (mainly due to the masking effects of dense vegetation covers) and (2) surfaces where the sensitivity of the SMOS TB observations to the surface effects can be clearly identified (the vegetation density is not sufficient to mask the surface emission). In a second step, over regions belonging to the second category, we attempted to compute maps of the roughness parameter (H_r). To that end, we used the retrieval method based on the TR parameter, combining the effects of the vegetation and roughness. First, TR and SM were retrieved simultaneously and at global scale from the SMOS L3 TB during 2011 by inverting the L-MEB model (L-band Microwave Emission of the Biosphere). Then, the effects of the vegetation and soil roughness included in the TR parameter were decoupled using a simple method described by Wang et al. (2015) to map the roughness parameter H_r at L-band.

The SMOS data and the other datasets used in this study are presented in Section 2, the L-MEB model and the simplification of the model by combining the soil roughness and vegetation effects are presented in the following section (Section 3). The latter section also presents the methodology used to compute the two maps: (1) the SMOS sensitivity to the surface effects and (2) the estimation of the soil roughness parameter (H_r) at global scale. Results and analysis of these maps are given in Section 4, followed by a discussion and conclusions in Section 6.

2. Data

2.1. SMOS Level 3 data

The SMOS mission is a joint program of the European Space Agency (ESA), the Centre National dEtudes Spatiales (CNES), and the Centro para el Desarrollo Teccnologico Industrial (CDTI) in the framework of the Earth Explorer Opportunity Mission initiative. It is the first satellite specifically dedicated to soil moisture retrievals with an L-band passive microwave radiometer at 1.4 GHz. SMOS has a sun-synchronous orbit at 757 km altitude with a 06:00 LST ascending equator crossing time and an 18:00 LST descending equator crossing time. The globe is fully imaged twice every three days. The main innovative feature of SMOS is the capability for multi-incidence-angle observations at full polarization across a 900 km swath. Acquisitions of brightness temperatures at different angles are made quasi-simultaneously over any location on the Earth.

In this study, the SMOS Level (L) 3 TB products (Al Bitar et al., in preparation) produced by the Centre Aval de Traitement des Données SMOS (CATDS) are used. These data are projected on the Equal-Area Scalable Earth (EASE) grid (Armstrong, Brodzik, & Varani, 1997) with a spatial resolution of 25 km × 25 km. The main differences between the SMOS L3 TB and the other lower levels of data are: (i) the L3 TB products are expressed at the top of the atmosphere over the terrestrial reference frame (H and V), and (ii) they are bin averaged from 2.5° to 62.5° every 5°. In this study, angles of incidence at 22.5° ± 2.5°, 32.5° ± 2.5°, 42.5° ± 2.5° and 52.5° ± 2.5° on ascending orbits of the SMOS L3 TB version 2.7 were considered to perform the SM and TR retrievals over the full globe during 2011.

Radio Frequency Interference (RFI) originating from man-made emissions in the protected/shared bands (i.e. satellite transmissions,

aircraft communications, radar, TV radio-links, FM broadcasts, and wireless camera monitoring systems) perturbs the natural microwave emission from the Earth's surface that is measured by passive microwave systems. These RFI have a significant impact on the TB at L-band (Oliva et al., 2012; Skou, Misra, Balling, Kristensen, & Sobjaerg, 2010). The SMOS L3 data were filtered to remove data contaminated by SMOS Radio Frequency Interference (RFI) by using amplitude limits and Stokes parameter limits but some low intensity RFI effects could still be present in the data. To remove these residual RFI effects as far as possible, quality control was applied to the SMOS L3 data by using the SMOS L3 SM flags and filtering out all the data where (i) DQX > 0.06 or (ii) DQX was equal to fill value or (iii) the probability of RFI was higher than 20% (Rodriguez-Fernandez et al., 2014; Wang et al., 2015). Retrievals cannot be computed over frozen soil. So, data obtained when the surface temperature was below 277 K were also filtered out (Parrens, Mahfouf, Barbu, & Calvet, 2014).

The auxiliary SMOS L3 data contain the percentage of nominal fraction (FNO) and forest fraction (FFO) for each pixel. In the operational SMOS retrieval algorithm, the SM and vegetation optical depth (τ_{nad}) retrievals are performed only over the nominal part. Over a pixel, this part is essentially composed of bare soil and low vegetation surfaces. The FFO is the percentage of forest present in a SMOS pixel. The FFO and FNO fractions are explained in detail in Kerr et al. (2012). In this paper, these quantities are used to analyze the soil roughness maps.

2.2. Other datasets

The surface soil temperature produced by the European Centre for Medium-range Weather Forecasting (ECMWF) for the top 0–7 cm from the surface was used in this study. This product was obtained by the SMOS L3 preprocessor, which computed the spatiotemporal average of the ECMWF forecast products on the EASE grid, and the soil texture was provided by the Food and Agriculture Organization at the SMOS spatial resolution (FAO, F., 1988).

To analyze the different maps computed here, the global land cover map from the Second Global Soil Wetness Project (GSWP2) was used (Dirmeyer et al., 2006). This map is based on the International Geosphere–Biosphere Programme (IGBP) classification system and contains twelve land cover biomes. The spatial resolution of the product is 1° and the data were re-scaled to the SMOS EASE grid (Fig. 1).

The digital elevation model obtained by the Shuttle Radar Topography Mission (SRTM) (Jarvis, Reuter, Nelson, & Guevara, 2008) with a spatial resolution of 30 arc sec (approximately 1 km) was also used to compute global elevation and topography slope maps. These data result from the Global 30 Arc-Second Elevation (GTOPO30) computed at the U.S. Geological Survey's EROS Data Center (USGS) and available at https://lta.cr.usgs.gov/GOTO30. The elevation map was computed by averaging all the SRTM elevation values present in a SMOS pixel while the topography slope map was computed by calculating the standard deviation of each SRTM elevation value present in a SMOS pixel.

The MODIS Leaf Area Index (LAI) data were also used to distinguish areas with low and high vegetation density and to create the H_r map. These data were obtained from the MCD15A2 products (MOD13A2, MCD15A2, U.R.O., Science (EROS) center, Sioux Falls, S.D., 2010). The spatial resolution of the product is 1 km. To be used in this study, it was re-scaled in the SMOS EASE grid following the methodology described in Lawrence et al. (2014). The mean values of LAI produced from the MODIS data over the full globe during 2011 are shown in Fig. 2.

3. Method

3.1. Overview and simplification of the $\tau-\omega$ model

The radiative transfer model used was the L-MEB model (Wigneron et al., 2007) implemented in the SMOS operational surface soil moisture retrieval algorithm (Kerr et al., 2012). The following presentation concentrates only on the basic principles of L-MEB as details of the model structure and parameterization have been given in several studies (Kerr, Waldteufel, Richaume et al., 2010; Wigneron et al., 2007). The L-MEB model is based on the $\tau-\omega$ model which is a widely recognized approach in the simulation of land surface emission using simplified (zero-order) radiative transfer equations (Jackson & Le Vine, 1996; Mo et al., 1982; Njoku et al., 2002; Wigneron, Chanzy, Calvet, & Bruguier, 1995). This model represents the soil as a rough surface in contact with a homogeneous vegetation layer. The brightness temperature can be expressed as a three-component model (Eq. (1)). The first part is the upward radiation from vegetation, the second is the downward emission from vegetation that is reflected by the soil and then attenuated by the canopy, and the last is the soil emission attenuated by the vegetation canopy.

$$TB_{(p,\theta)} = (1-\omega_p)\left(1-\gamma_{(p,\theta)}\right)T_c\gamma_{(p,\theta)}r_{G(p,\theta)} + (1-\omega_p)\left(1-\gamma_{(p,\theta)}\right)T_c + (1-r_{G(p,\theta)})\gamma_{(p,\theta)}T_G \quad (1)$$

where T_G and T_C are the effective soil and vegetation temperatures, respectively. r_G is the soil reflectivity, ω_p is the effective scattering albedo accounting for the effects of canopy volume scattering (Kurum, 2013) and γ is the vegetation attenuation factor. p and θ are the polarization and the incidence angle of the observations. Van de Griend and Owe (1994), Mladenova et al. (2014), and Njoku and Chan (2006) showed that the ω_p had only slight effects on the range of the radiation emitted from vegetated surfaces at microwave wavelengths. For simplicity, in this study, we set ω_p equal to zero (Jackson, 1993; Njoku & Chan, 2006; Parrens et al., 2016; Van de Griend & Owe, 1994; Wang et al., 2015). Furthermore, we assumed that the effective soil and vegetation temperatures were equal and represented by T. This

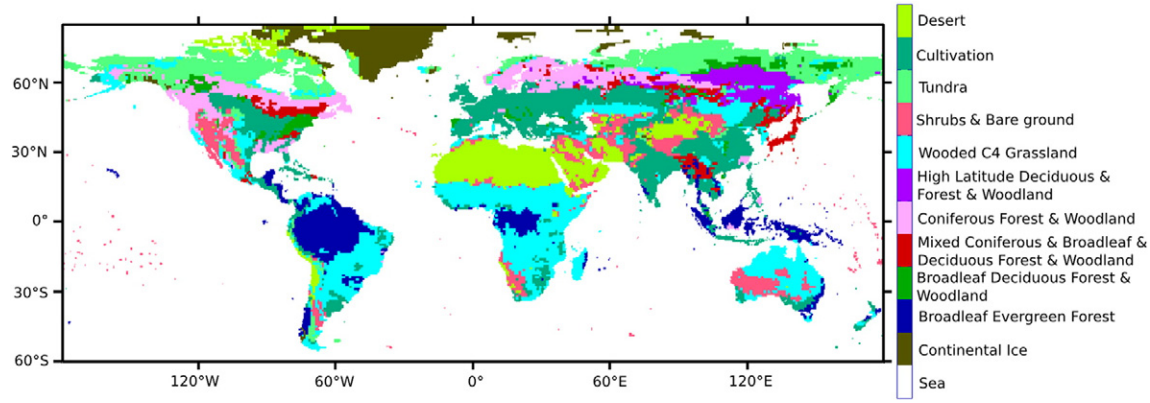

Fig. 1. Distribution of the major vegetation biomes in accordance with Dirmeyer et al. (2006).

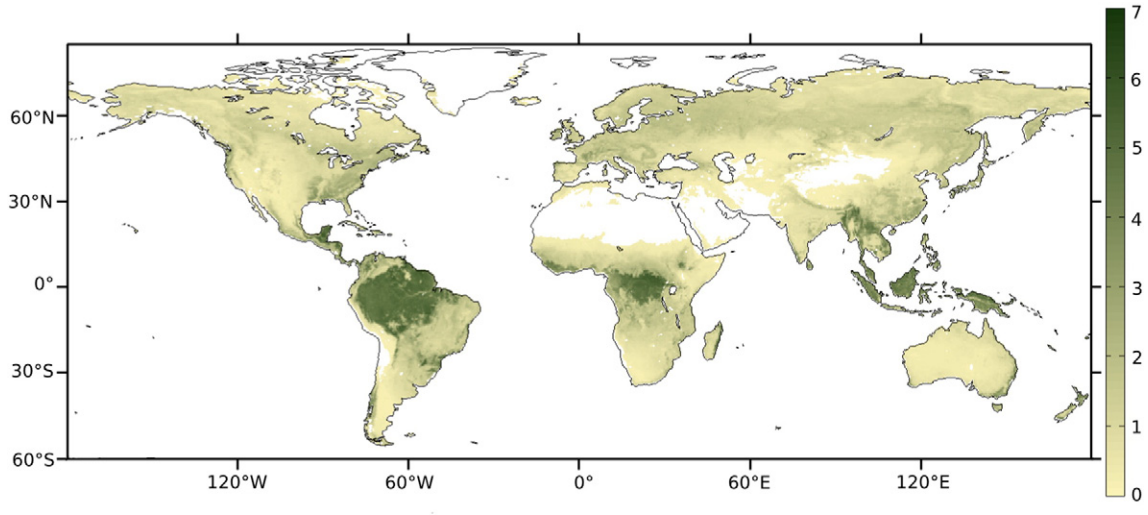

Fig. 2. Mean LAI values obtained from MODIS data for 2011.

assumption is reasonable at 6 a.m (Jackson, 1980; Parrens et al., 2016). These assumptions led to the following simplified equation:

$$TB_{(p,\theta)} = T\left[1-\gamma^2_{(p,\theta)} r_{G(p,\theta)}\right]. \quad (2)$$

To model the soil reflectivity, the L-MEB model is based on a semi-empirical approach which has been tested against experimental data sets at L-band (Escorihuela et al., 2007; Saleh et al., 2007; Wigneron et al., 2001, 2007, 2011). The approach was initially developed by Wang and Choudhury (1981) and Wegmuller and Matzler (1999) and the N_{rp} parameter was included in the soil roughness modeling in a second step. The roughness modeling is based on four roughness parameters (H_r, Q_r and N_{rp}) and smooth soil reflectivity ($r_{G(p,\theta)}$). The p-polarized soil reflectivity ($r_{G(p,\theta)}$) is given by:

$$r_{G(p,\theta)} = \left[(1-Q_{(p,\theta)}) r^*_{G(p,\theta)} + Q_{(p,\theta)} r^*_{G(p,\theta)}\right] \exp\left(-H_r \cos^{N_{rp}}(\theta)\right). \quad (3)$$

$r^*_{G(p,\theta)}$ is calculated from the soil permittivity value by applying the Fresnel equations (Ulaby, 1982). The soil permittivity depends on the properties of the soil, including the soil moisture content. Several models are available to calculate this value. In this study, the soil permittivity was computed with the Mironov model, which is currently used in the SMOS operational retrieval algorithm (Mironov, Kerr, Wigneron, Kosolapova, & Demontoux, 2013). This model computes the soil permittivity as a function of the soil clay content (%), the soil temperature and the soil moisture content. H_r is an effective roughness parameter that accounts for (1) geometric roughness effects, in relation with the spatial variations in the soil surface height and (2) dielectric roughness effects in relation with the spatial variations in the dielectric constant at the soil surface and within the soil, which can be caused by non-uniformities in the soil characteristics (soil moisture content, texture, density, etc.) (Escorihuela et al., 2007; Saleh et al., 2006; Wigneron et al., 2001). At L-band wavelengths, the H_r value ranges from ~0 (for smooth surfaces) to ~1 (for very rough soils) (Wigneron et al., 2001). The N_{rp} parameters are used to account for angular effects on the soil reflectivity that are due to surface roughness. In the literature, there is no clear consensus on the value of this parameter. The values used for N_{rp} generally vary from −1 to 2 (Escorihuela et al., 2007; Saleh et al., 2007; Wigneron et al., 2001, 2007, 2011). In this study, following the results obtained by Lawrence et al. (2013), the values of N_{rp} for the two polarizations were set equal ($N_{rH} = N_{rV}$). In L-MEB, the Q_r parameter accounts for polarization mixing effects. Wang, O'Neill, Jackson, and Engman (1983) found that small values for Q_r were obtained in the L-band. This is in agreement with most of the published studies based on large experimental data sets (Escorihuela et al., 2007; Montpetit et al., 2015; Saleh et al., 2007; Wigneron et al., 2001, 2007, 2011) and we considered, here, that $Q_r = 0$.

The vegetation attenuation factor due to the canopy, also referred to as transmissivity, depends on the angle of incidence and the polarization. It is expressed as:

$$\gamma_{(p,\theta)} = \exp\left(\frac{-\tau_{nad}\left(\cos^2(\theta) + tt_p \sin^2(\theta)\right)}{\cos(\theta)}\right). \quad (4)$$

τ_{nad} is the optical depth at nadir (i.e. $\theta = 0^\circ$) and it is independent of both the angle of incidence and the polarization. tt_p is a specific vegetation parameter accounting for the effect of the vegetation structure on the angular dependence of τ_{nad}. We assumed that $tt_H = tt_V = 1$. This corresponds to isotropic conditions, where the optical depth of the standing canopy is assumed to be independent of both polarization and angle of incidence. Considering that, at coarse spatial resolution, the pixel includes a variety of vegetation types, the effects related to the structure of a variety of vegetation canopies are mixed together, so it is reasonable to assume that the optical depth is polarization-independent ($tt_H = tt_V = 1$) (Mladenova et al., 2014; Owe et al., 2001; Van de Griend & Owe, 1994).

As mentioned in the Introduction, the present study is based on the simultaneous retrievals of SM and TR (parameter combining the effects of surface roughness and vegetation). This method has been used in several studies in the literature (Bindlish et al., 2003; Jackson, Hsu, & O'Neill, 2002; Njoku & Chan, 2006; Saleh et al., 2006; Schmugge, Jackson, Kustas, & Wang, 1992). At L-band, the combination of the vegetation and roughness effects in the L-MEB model was analyzed in detail by Bindlish et al. (2003), Fernandez-Moran et al. (2015), Jackson et al. (2002), Njoku and Chan (2006), Saleh et al. (2006), and Schmugge et al. (1992).

By combining Eqs. (2), (3) and (4), TB at a given angle of incidence and polarization can be expressed as:

$$TB_{(p,\theta)} = T\left[1-r^*_{G(p,\theta)} \exp\left(\frac{-2\tau_{nad}}{\cos(\theta)} - H_r \cos^{N_{rp}}(\theta)\right)\right]. \quad (5)$$

Based on a previous study (Parrens et al., 2016), N_{rp} was set to −1 to combine the vegetation and roughness effects in a single parameter (TR). Note that, in the past, several studies (Cano et al., 2010; Escorihuela et al., 2007; Saleh et al., 2007; Schlenz et al., 2012;

Wigneron et al., 2007, 2012) have also set this parameter to −1. The combined vegetation and roughness parameter is expressed as:

$$TR = \tau_{nad} + \frac{H_r}{2} \quad (6)$$

and the radiative transfer model (Eq. (1)) can be simplified to:

$$TB = T\left[1 - r^*_{G(p,\theta)} \exp(-2TR/\cos(\theta))\right]. \quad (7)$$

Note that, when simultaneous retrievals of SM and TR are made, there is no need to calibrate the H_r parameter (as it is implicitly accounted for in TR).

3.2. The retrieval process

In this study, the simplified radiative transfer model combining the roughness and the vegetation effects (Eq. (7)) was inverted to retrieve SM and TR over the whole globe during the year 2011. The retrievals were made when at least six observations were available, including both polarizations and at least three angles of incidence among the following four values available in the Level 3 TB data set: $22.5^\circ \pm 2.5^\circ$, $32.5^\circ \pm 2.5^\circ$, $42.5^\circ \pm 2.5^\circ$ and $52.5^\circ \pm 2.5^\circ$. The model inversion was based on minimizing the following cost function (C_F):

$$C_F = \frac{\sum\left(TB^o_{(\theta,p)} - TB^s_{(\theta,p)}\right)^2}{\sigma^2_{TB}} + \frac{\sum_i (p_i - p_i^{init})}{\sigma^2_p}. \quad (8)$$

The cost function (Eq. (8)) includes the classical cumulative squared difference between the simulated and observed brightness temperatures (TB^s and TB^o, respectively) normalized by the uncertainties in the first term of the equation and the additional terms that account for the squared difference between the current value (p_i) and the initial guess (p_i^{init}) of each SM and TR variable were $\sigma_{p,SM} = 0.02$ m^3 m^{-3} and $\sigma_{p,TR} = 0.05$ respectively. These values are of the same order of magnitude as those used in the literature (Cano et al., 2010; Wigneron et al., 2007). The standard deviation of the TB measurements was set equal to $\sigma_{TB} = 2.5$ K in accordance with Wigneron et al. (2007). The TB observations were taken to be independent, considering the technical specifications for the design of the SMOS antenna. The initial values for the retrieved parameters SM and TR were set equal to 0.2 m^3 m^{-3} and 0.2, respectively (Wigneron et al., 2011).

3.3. Computing the global roughness maps

3.3.1. General approach

A general scheme of the approach we used to compute the H_r parameter at global scale is given in Fig. 3. Three main steps can be distinguished in the general approach:

1. First, we considered pixels where there was bare soil and/or sparse vegetation cover over a sufficient period of time (case 1 corresponding to bare soil and/or sparsely vegetated surfaces) and pixels where there was vegetation cover all the time (case 2 corresponding to vegetated surfaces). The "sufficient period of time" was defined here by a minimum of 40 observation dates and a threshold value of LAI equal to 0.5 m^2 m^{-2}. More specifically, pixels for case 1 were

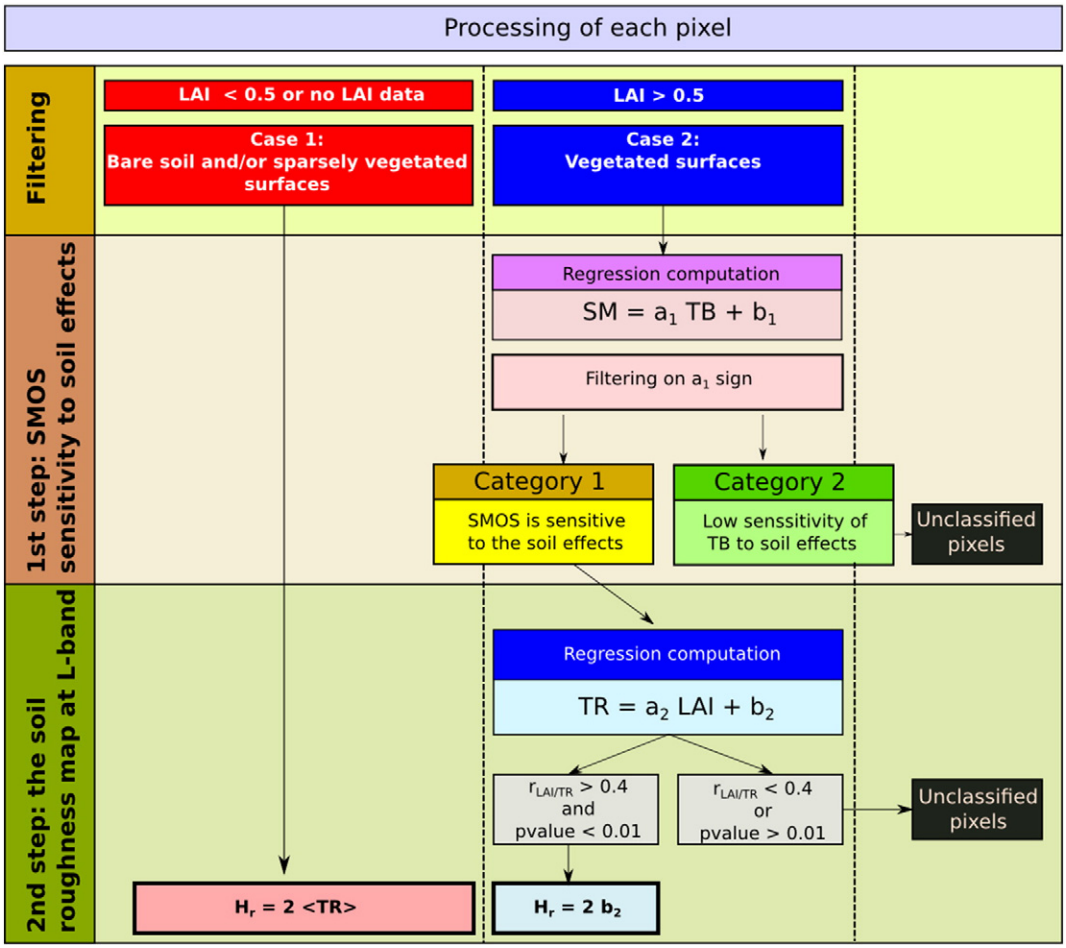

Fig. 3. Summary of the methodology used to compute the maps of the H_r parameter.

selected as pixels where the LAI data were lower than 0.5 m^2 m^{-2} for at least 40 observation dates, while the pixels that did not satisfy this condition were considered as case 2.
2. Second, for vegetated pixels corresponding to case 2, we distinguished between pixels where the SMOS observations were sensitive to the surface effects (defined here as category 1) and pixels where there was a very low sensitivity of the SMOS observations to the surface microwave emission (defined here as category 2). Over the pixels corresponding to the latter category, no H_r retrieval could be carried out and the pixels were considered as unclassified pixels.
3. Third, over pixels corresponding to category 1 or case 1, 2-parameter retrievals of SM and TR (parameter accounting for the combined effects of vegetation and surface roughness) were performed over the whole globe, except over areas where RFI probability was higher than 20%. Then, vegetation and roughness effects were decoupled to compute the H_r parameter.

More details about this general approach for steps 2 and 3 are given below.

3.3.2. Mask of the SMOS sensitivity

Over some pixels (such as pixels with dense vegetation), the soil emission signal is almost totally masked by the vegetation layer. We attempted to compute a map locating pixels where the SMOS observations were sensitive to the surface effects and pixels where there was very low sensitivity of the SMOS observations to the soil microwave emission. In this study, we considered that, over pixels covered by bare soil and/or sparsely vegetated surfaces (case 1), SMOS was sensitive to the surface effects (Kerr et al., 2001). Over the vegetated pixels corresponding to case 2 (where 40 observation dates corresponding to low vegetation conditions, i.e. LAI lower than 0.5 m^2 m^{-2} were not available), the following regression equations, as defined by Eq. (9), were used:

$$SM = a_1(p,\theta)TB(p,\theta) + b_1(p,\theta) \quad (9)$$

where $a_1(p,\theta)$ is the slope parameter and expresses the variations of SM with respect to the variations of TB, and $b_1(p,\theta)$ is the intercept parameter. Eight regressions were performed over the full globe for the different values of the angle of incidence (θ) ($22.5^\circ \pm 2.5^\circ$, $32.5^\circ \pm 2.5^\circ$, $42.5^\circ \pm 2.5^\circ$ and $52.5^\circ \pm 2.5^\circ$) and the two polarizations (p = H or V). It is well known that an increase in SM leads to a decrease in the TB values (Schmugge, 1983; Ulaby, 1982; Wigneron et al., 2001). So, positive values of $a_1(p,\theta)$ were interpreted as a sign of very low sensitivity of TB to the soil surface effects. For a given pixel, if all the slope parameters of the eight regression equations had a negative value, we considered that SMOS was sensitive to the surface effects over this pixel (case corresponding to category 1). Conversely, for a given pixel, if at least one of the slope parameters of the eight regression equations had a positive value, we considered that SMOS observations had very low sensitivity to the surface effects over this pixel (case corresponding to category 2). Note that (results not shown), when one of the values of $a_1(p,\theta)$ was positive, in general, all the values of $a_1(p,\theta)$ for the different values of incidence angle and the two polarizations were positive. Moreover, if the correlation value (r) between SM and TR was lower than 0.4 or the p-value was higher than 0.01, we consider very low sensitivity of the SMOS observations to the surface effects over this pixel (category 2).

Following this methodology, a mask of the SMOS soil sensitivity to the surface effects was computed.

3.3.3. Soil roughness maps

The computation related to the soil roughness map was made only over the pixels corresponding to case 1 (corresponding to bare soil and/or sparsely vegetated surfaces) and over vegetated pixels belonging to category 1 (as defined in the section above), i.e. pixels, where the sensitivity of the SMOS observations to the surface effects was not negligible. MODIS LAI data were used to decouple the vegetation and the surface roughness effects in the TR parameter as proposed by Wang et al. (2015). To compute the H_r value of each pixel, the main cases 1 and 2 were considered following the values of the MODIS LAI over the pixel in 2011 (a threshold value of LAI equal to 0.5 m^2 m^{-2} was considered in this study).

- Pixels corresponding to case 1 (bare and/or sparsely vegetated surfaces):
  For case 1, a direct inversion of H_r was carried out over the time period when LAI < 0.5 m^2 m^{-2}, assuming vegetation effects could be neglected (TR $\approx H_r/2$). So, if at least forty 2-parameter (SM and TR) retrievals could be made for dates corresponding to LAI < 0.5 m^2 m^{-2}, 2, we considered that H_r was equal to the average values of 2 × TR over the retrieval period.
- Pixels corresponding to both case 2 & category 1 (vegetated surfaces where the SMOS sensitivity to the surface effects cannot be neglected):
  In this case, the vegetation effects (parameterized by the τ_{nad} parameter) could not be neglected. To decouple the vegetation effects (through the τ_{nad} parameter) and the roughness effects (through the H_r parameter), we considered the approach developed by Wang et al. (2015). Wang et al. (2015) considered that the vegetation optical depth could be linearly related to the LAI index. This assumption was used in the SMOS L2 operational algorithm and analyzed by Wigneron et al. (2007) and Lawrence et al. (2014). Note that this linear assumption is an approximation. For example, over regions of crops in the USA, Lawrence et al. (2014) showed that τ_{nad} and LAI values started to increase at the same time but with τ_{nad} reaching a peak later than LAI. This behavior can decrease the linear link between LAI and τ_{nad}. However, the linear link between LAI and τ_{nad} is a good approximation in general and, assuming roughness effects to be constant over a given pixel, we assumed that TR could be expressed as a function of LAI over each pixel as:

$$TR = a_2 \mathrm{LAI} + b_2 \quad (10)$$

where a_2 is the slope parameter and b_2 the intercept parameter. In this case, the H_r parameter can be related to the intercept parameter (b_2) of the regression equation (Eq. (10)) (we assumed that, at the intercept, corresponding to LAI = 0, the optical depth $\tau_{nad} = 0$). If τ_{nad} can be neglected for LAI = 0, H_r can be written as: $H_r = 2\ b_2$. Note that this method was applied only if the correlation value (r) between LAI and TR was higher than 0.4 and if a significant p-value (p-value < 0.01) associated with the regression equation was obtained.

4. Results

This section is divided into three parts: the first concerns the SM and TR retrievals obtained during 2011. The second concerns the analysis of the SMOS sensitivity to the surface effects and the third focuses on the mapping of the soil roughness effects.

4.1. SM and TR retrievals

Based on the approach defined above (see Fig. 3), a map distinguishing pixels corresponding to case 1 (bare and/or sparsely vegetated surfaces, corresponding to values of LAI < 0.5 m^2 m^{-2} during at least 40 days) and case 2 (when conditions for case 1 were not fulfilled, corresponding roughly to vegetated surfaces) is shown in Fig. 4. At a global scale, 39% of the pixels correspond to case 1 and 61% to case 2.

The 2-parameter retrievals of SM and TR retrievals were carried out globally. For case 1, direct values of H_r were derived from the retrieved

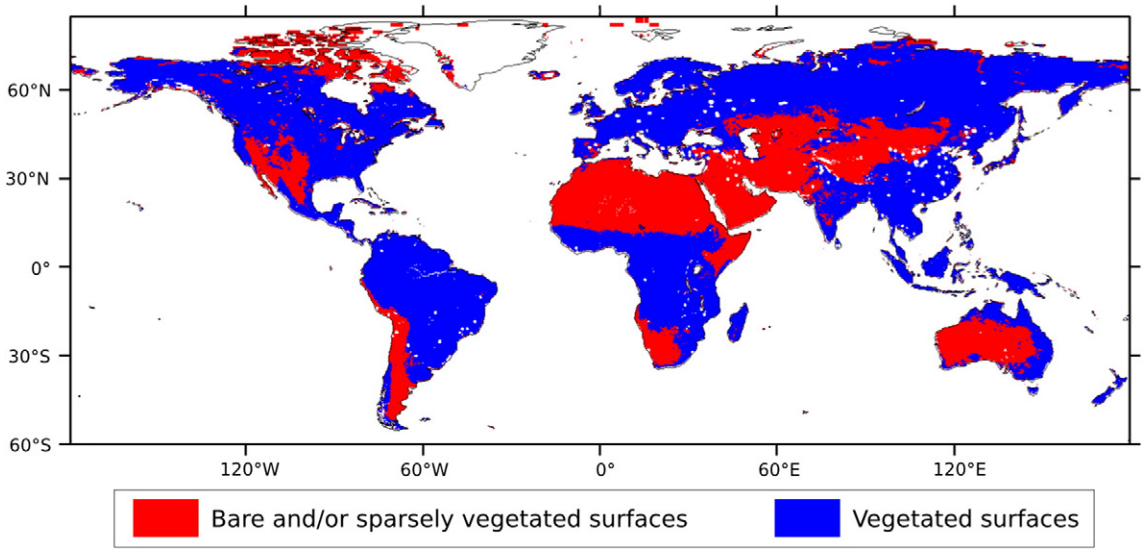

Fig. 4. Spatial distribution of the bare and/or sparsely vegetated surfaces (red), corresponding to case 1, and vegetated surfaces (blue), corresponding to case 2. (For interpretation of the references to color in this figure legend, the reader is referred to the web version of this article.)

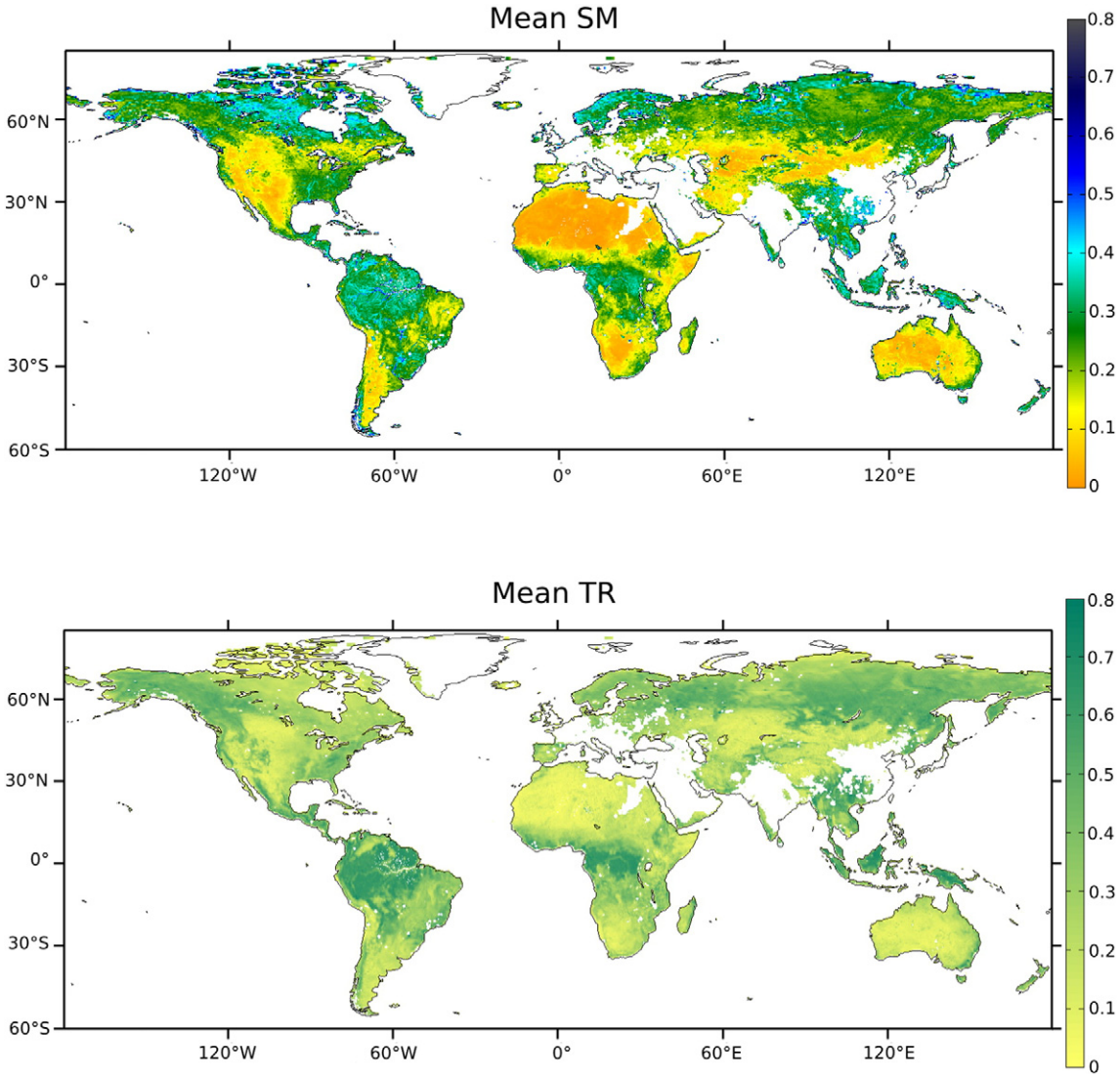

Fig. 5. Mean values of SM (top) and TR (bottom) retrievals obtained during 2011.

values of TR. For case 2, the SM retrievals were used to classify the pixels in categories 1 & 2.

Fig. 5 shows the mean of SM and TR retrievals obtained by combining the roughness and vegetation effects during the year 2011 for the whole globe. Pixels where the RFI probability was higher than 20% were filtered out in these maps. Mean SM retrieval values during 2011 range from 0 to 0.60 $m^3\ m^{-3}$. The drier part of the globe is located in the north and south of Africa and the middle of Australia. To a lesser extent, the eastern part of North America, the southern part of South America and the Eurasian and mid-Asian continent are also dry with mean SM values ranging between 0.05 $m^3\ m^{-3}$ and 0.15 $m^3\ m^{-3}$. The wetter part of the globe corresponds to the Amazon area, the northern regions of Europe, the south of continental Asia and the Indonesian islands. The median value of SM for the whole globe during 2011 is 0.175 $m^3\ m^{-3}$ and the standard deviation of SM is equal to 0.047 $m^3\ m^{-3}$. These results have already been evaluated against in situ data in previous studies (Fernandez-Moran et al., 2015; Parrens, Wigneron et al., 2014).

The mean value of the combined roughness–vegetation (TR) parameter ranges between 0 and 0.7 over the whole globe. The higher values of TR can be observed over the north of Russia, the middle of South America, Africa and Alaska. Conversely, the lower values of TR can be seen over the African deserts, the middle of Australia and Eurasian and middle Asia. The median and the standard deviation values of TR retrievals for all the continents during 2011 are 0.22 and 0.13, respectively. The major rivers are particularly visible in the mean TR retrievals over the Amazon and Congo basins.

4.2. Mask of SMOS sensitivity to the surface effects

The regression coefficients (a_1 and b_1) over the globe obtained with Eq. (9) between SM and TB at H polarization at $40^\circ \pm 5^\circ$ of angle of incidence are shown in Fig. 6. The slope parameter a_1 ranges from $-0.0151\ m^3\ m^{-3}/K$ to $0.0055\ m^3\ m^{-3}/K$. As explained in the previous section, a positive value of the a_1 parameter is a sign indicating very low sensitivity of the SMOS observations to the surface effects. At H-pol and at 40° of incidence, we can observe positive values of a_1 over dense tropical forests and in northern regions. For example, positive values of a_1 were found in the Amazon and Congo forests, indicating that SMOS sensitivity to the surface effects was very low. As for the b_1 parameter of the regression, values range from 0 $m^3\ m^{-3}$ to 4.4 $m^3\ m^{-3}$. Note that the white areas correspond to pixels where no computations were done due to a high RFI probability (RFI probability higher than 20%). The same regression equations between TB and SM were applied for the other angles of incidence and the H and V polarizations. Similar

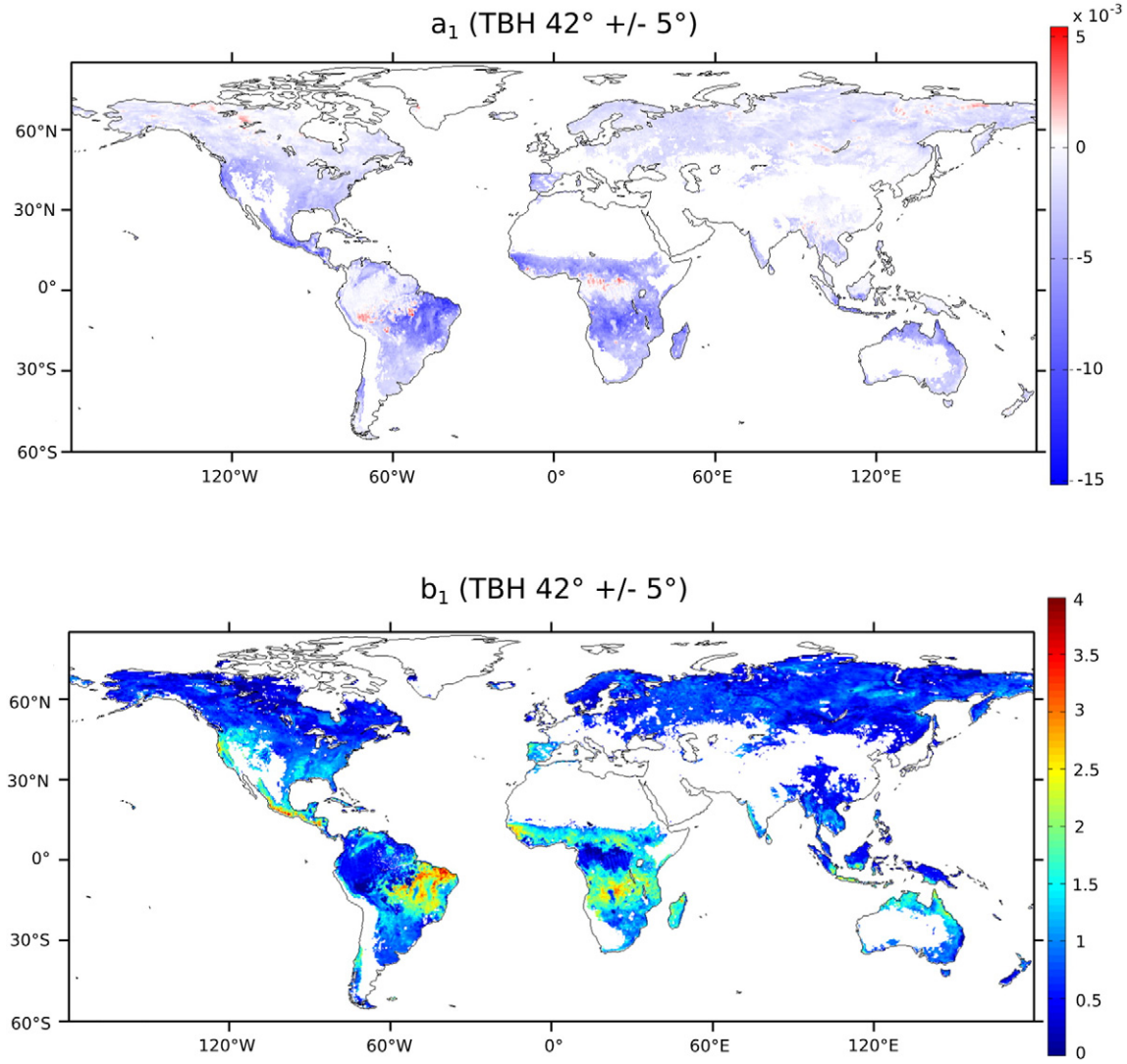

Fig. 6. Global maps of the regression coefficients computed from Eq. (9). This regression was performed with TB values at H polarization and angle of incidence of $42^\circ \pm 5^\circ$. Note that the computation of the regression coefficients done in this figure concerns only the pixels considered as "vegetated" (pixels in blue in Fig. 4). (For interpretation of the references to color in this figure legend, the reader is referred to the web version of this article.)

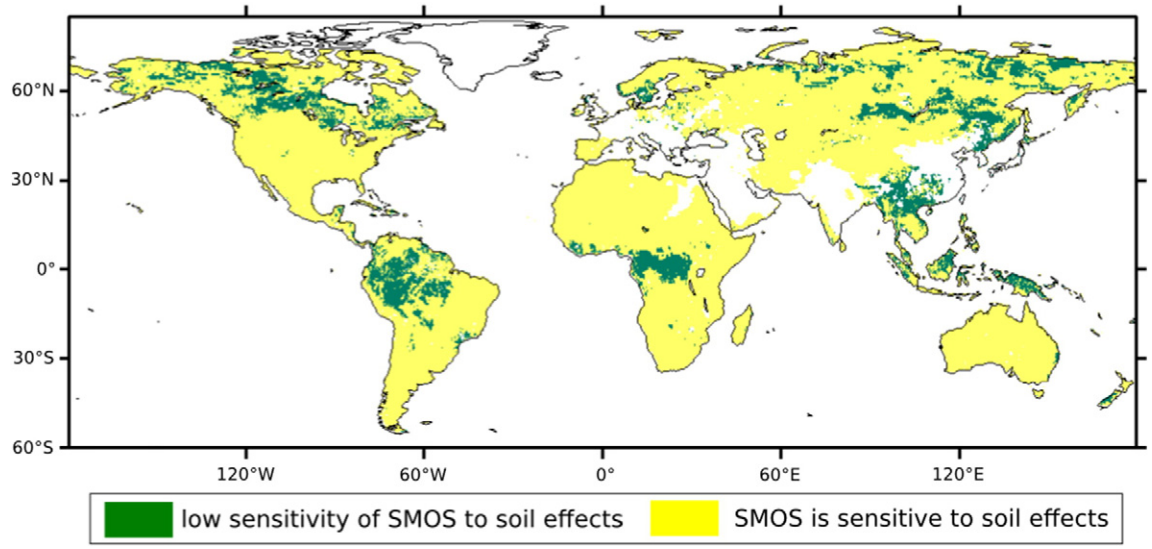

Fig. 7. Global maps of the pixels where SMOS TB is sensitive to the surface effects (yellow), corresponding to case 1 and category 1, and areas where the sensitivity of SMOS TB to the surface effects is very low or negligible, corresponding to category 2 (green). Masked areas in white correspond to pixels with an RFI probability higher than 20%. (For interpretation of the references to color in this figure legend, the reader is referred to the web version of this article.)

results to those found at H-pol and $\theta = 40^{\circ} \pm 5^{\circ}$ were obtained (results not shown).

Fig. 7 presents the global map showing the pixels where (i) the SMOS observations are sensitive to the surface effects, i.e. pixels correspond either to case 1 (bare and/or sparsely vegetated surfaces) or to category 1 (vegetated pixels where a sensitivity of TB to SM could be revealed); and (ii) pixels where SMOS sensitivity to the surface effects is very low. The latter condition corresponds to category 2 or to pixels where the correlation value between SM and TB is lower than 0.4 or the p-value is higher than 0.01. RFI effects (where the RFI probability is higher than 20%) were filtered out in these maps and showed as blank areas. It was found that the SMOS observations were sensitive to the surface effects over 87% of the continental surface of the globe. SMOS sensitivity to the ground surfaces is very low for 13% of the globe, in particular over equatorial forests and regions of tundra.

A more detailed analysis of the pixels where SMOS was sensitive to the surface effects was carried out with respect to the vegetation type. Fig. 8 shows the percentage of pixels where the SMOS observations were found to be sensitive to the surface effects (red bars) and where SMOS sensitivity was low (black bars) with respect to the vegetation types as defined by Dirmeyer et al. (2006). The sensitivity of the SMOS observations (TB) to the surface effects was found to depend on the vegetation type. For example, over broadleaf evergreen forests, the SMOS observations were sensitive to the surface effects for only 50% of the pixels covered by this vegetation type. Conversely, over wooded C4 grasslands, SMOS was sensitive to the surface effects for 95% of the pixels. The SMOS observations were sensitive to the surface effects for more than 80% of the pixels over (i) broadleaf deciduous forest and woodland, (ii) coniferous forest and woodland, (iii) wooded C4 grasslands, (iv) tundra and (v) cultivation. They were sensitive to the

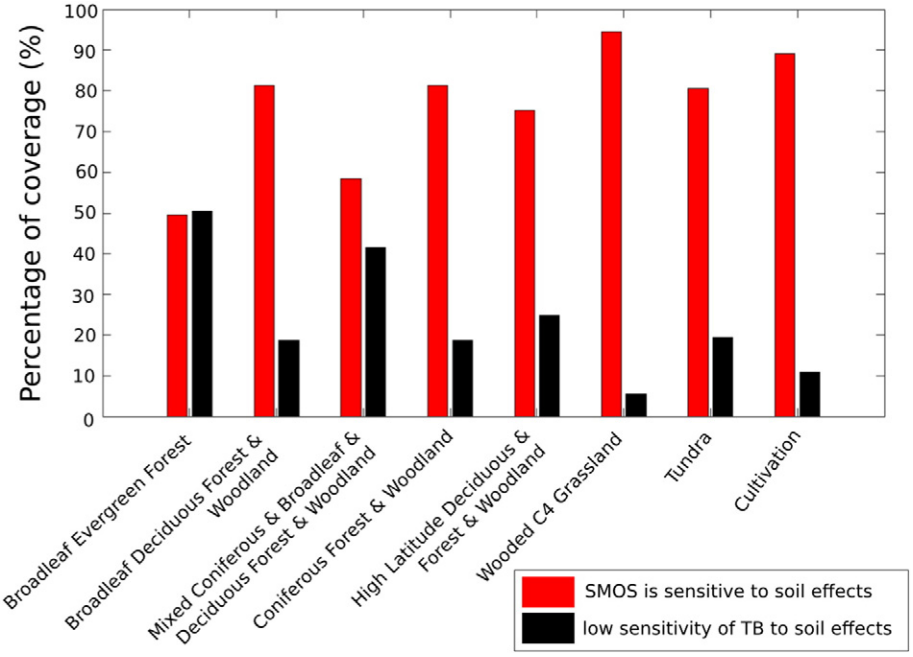

Fig. 8. SMOS sensitivity to the surface effects with respect to the major vegetation biomes as defined in Dirmeyer et al. (2006). (For interpretation of the references to color in the text, the reader is referred to the web version of this article.)

surface effects over 55%–75% of the pixels for the (i) mixed coniferous and broadleaf and deciduous forest and woodland and (ii) high latitude deciduous forest and woodland. SMOS observations were also sensitive to the soil surfaces over 100% of the pixels for deserts, bare soils and shrub vegetation types, which are not represented in Fig. 8.

This mask (Fig. 7) is used in the following section to filter out all the pixels where sensitivity of TB to the surface effects is very low.

4.3. Surface roughness effects as seen by SMOS

Over pixels where the SMOS TB data were found to be sensitive to the surface effects (case 1 or category 1), the value of the H_r parameter was computed as summarized in Fig. 3. For case 1, direct values of H_r were derived from the retrieved values of TR. For pixels corresponding to both case 2 and category 1, the values of H_r were computed from the value of the intercept of the relationship between TR and LAI. For pixels corresponding to both case 2 and category 2, no retrievals could be made and the pixel was considered as unclassified.

Fig. 9 shows the temporal correlation values (correlation coefficient, r) obtained between the MODIS LAI data and the TR retrievals during 2011. The value of the correlation coefficient between LAI and TR over the globe follows a normal distribution with a mean value equal to 0.42 and a standard deviation value equal to 0.15. The minimum value of r is equal to -0.87 whereas the maximum value is 0.81. Over the globe, a negative correlation between LAI and TR is obtained over 11% of the pixels. For these pixels, the MODIS LAI data present a dynamic seasonal evolution whereas the TR retrievals do not present a seasonal cycle. Low correlation values ($0 < r < 0.4$) are obtained over 18% of the pixels. These pixels are generally composed of different vegetation types: cultivated land, tundra, shrubs and bare ground, wooded C4 grassland and forests (coniferous and deciduous). Higher correlation values ($0.4 < r < 0.81$) between LAI and TR retrievals are obtained over the eastern part of North America, the eastern part of South America, the south of the Sahara desert, the south of Africa, the east of the Congo forest, the west coast of Australia and the eastern part of Australia.

The method used to compute the global map of the roughness parameter (H_r) is illustrated in Fig. 10. In Fig. 10a the method was used for bare or sparsely vegetated surfaces (corresponding to case 1) over a pixel located in the Sahara desert (24.08°N,8.30°E). More than forty TB observation data for LAI lower than 0.5 m^2 m^{-2} were available, so the mean of TR retrievals could be computed and set equal to $H_r/2$. The value obtained for H_r is equal to 0.024. Fig.10b illustrates the method developed for vegetated surfaces (category 1). This figure shows the TR retrievals as a function of LAI data for a pixel located in the eastern part of the US (40.98°N, 89.80°W). The correlation value and root mean square value (RMSE) between TR and LAI values are 0.81 and 1.49, respectively. The slope parameter of this regression is equal to 0.082 m^2 m^{-2} and the intercept, corresponding to the value of $H_r/2$, is equal to 0.14.

Using the same approach as the one illustrated above for the two selected pixels, the values of H_r were estimated at global scale for all pixels corresponding to case 1 and to category 1 and are shown in Fig. 11. No discontinuities in the H_r values can be noted in the global map between the two different approaches considered for case 1 and for category 1. In Fig. 11, it can be seen that the lowest values of H_r were obtained in deserts or in low vegetated regions (i.e. Sahara desert, Australia, southern Africa). Note that at C-band, Pellarin et al. (2009) found a wider diversity of soil roughness effects due to topography (dunes, flat areas, plains) in Sahel and Sahara areas. In the results obtained at L-band (Fig. 11), it seems that the topographic effects do not lead to a high variability of H_r in these regions. Conversely, the highest values of H_r were obtained in forested areas and in the northern regions of the globe. These results are in accordance with those found by Wang et al. (2015) at C-band.

The values of H_r were analyzed according to the different types of vegetation. The average value of H_r computed for each type of vegetation is shown in Fig. 12. For each vegetation biome, at least 4910 pixels were considered to compute the average. The mean value of H_r ranges between 0.14 (lowest values obtained over deserts) and 0.39 (highest values obtained over high latitude deciduous forest and woodland). It can be seen that H_r is generally higher over forest biomes (broadleaf evergreen forest, broadleaf deciduous forest, mixed coniferous forest and coniferous forest), with values ranging from 0.32 to 0.39. Presently, the higher H_r values obtained over forest biomes cannot be totally explained. Future investigations are needed. In the literature, H_r values over forest biomes are close to 0.3 (Ferrazzoli, Guerriero, & Wigneron, 2002; Rahmoune et al., 2014). In our study, the retrieved H_r values range between 0.32 and 0.39 and are consistent with the literature. It is likely that the higher values of H_r can be explained by the presence of ground litter under the forest canopy. The litter tends to increase the H_r value, which acts as an effective parameter accounting for both soil roughness and ground litter (Grant et al., 2007, 2008; Saleh et al., 2006). Lower values of H_r were obtained over wooded C4 grassland, tundra and cultivated areas. Over these biomes, the H_r values range between 0.20 and 0.23. The lowest values of H_r can be noted over shrubs, bare soils and deserts (with values around 0.14–0.16).

As shown before, the value of H_r depends on the vegetation type but some other factors can also influence the H_r values. Because of the coarse spatial resolution (25 km × 25 km) of the SMOS microwave

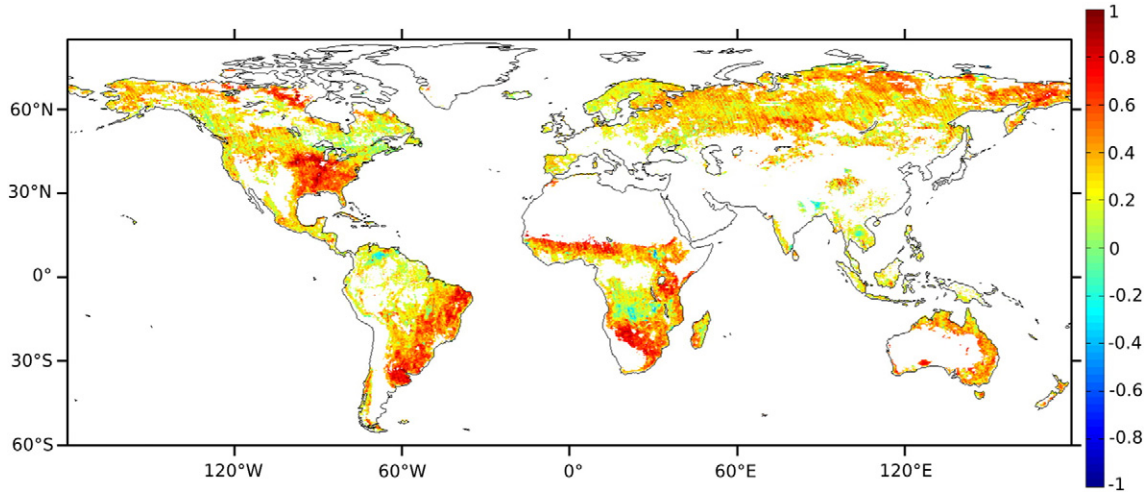

Fig. 9. Temporal correlation (r) values obtained between MODIS LAI data and TR retrievals for 2011.

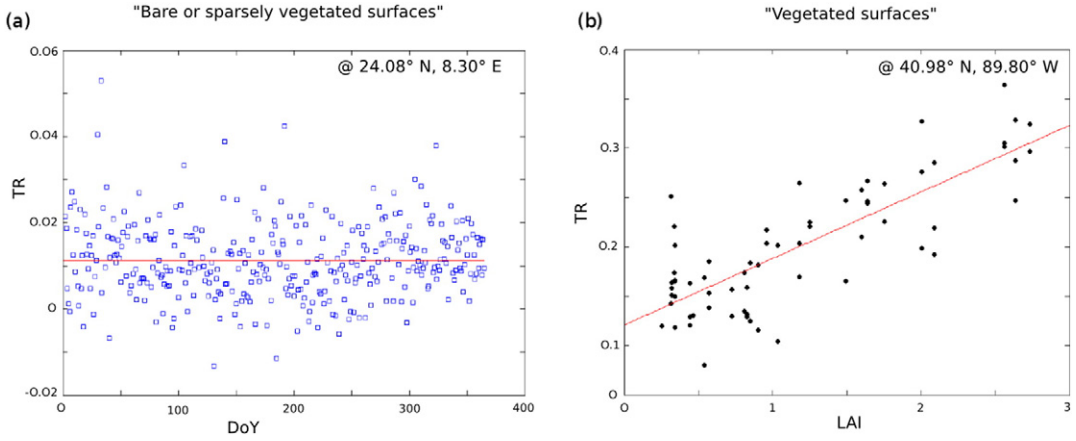

Fig. 10. Illustration of the method described in Section 3 and used to compute the soil roughness map for (a) case 1 (bare and/or sparsely vegetated surfaces): TR retrievals obtained for one pixel (24.08°N,8.30°E) during the full year 2011. The red line represents the mean of the TR values and corresponds to the H_r value (b) case 2 and category 1 (vegetated pixel): Scatter plot between TR retrievals and LAI MODIS data for one pixel (40.98°N,89.80°W). For vegetated surfaces, the H_r value corresponds to the intercept of the regression. (For interpretation of the references to color in this figure legend, the reader is referred to the web version of this article.)

observations at L-band, the measured signal can be affected by many features, such as the topography and the percentage of forest and nominal fraction in each pixel. In this study, we analyzed the value of H_r with respect to the FFO (percentage of the forest fraction present in one SMOS pixel), FNO (percentage of the nominal fraction present in one SMOS pixel), the mean LAI, the altitude and the topography slopes. At global scale, without making distinction between biomes, the spatial correlations between H_r values and FFO, FNO, LAI, altitude and the topography slopes were equal to 0.58, −0.52, 0.56, 0.06 and 0.27, respectively. So, at global scale, it seems that the values of H_r can be explained mainly by the presence of vegetation (parameterized here by FFO, FNO and LAI), while the effects of the altitude and the topography slopes are very small.

Fig. 13 shows the correlation values (r) between H_r and FFO, FNO, mean LAI, altitude and the topography slopes according to the vegetation biomes. Concerning the spatial correlation between H_r and FFO, the highest correlation ($r = 0.58$) values are obtained for the vegetation biomes composed of wooded C4 grassland while the lowest correlation value ($r = 0.15$) is obtained over the desert. For the correlation between FNO and H_r, all the correlation values are negative: an increase in the FNO percentage leads to a decrease in the H_r value. The highest correlation value in absolute terms ($r = -0.57$) was obtained for the wooded C4 grassland biome. A very low correlation of the values of H_r and FNO ($-0.2 < r < 0$) was found over three biomes: (i) mixed coniferous and broadleaf and deciduous forest and woodland, (ii) high latitude deciduous forest and woodland and (iii) tundra. Correlation (r) values were also computed between LAI and H_r. The three highest values of correlation ($r < 00.4$) corresponded to (i) wooded C4 grassland, (ii) tundra and (iii) broadleaf evergreen forest (in descending order). Very low correlation values ($0 < r < 0.2$) were obtained for shrubs and bare ground, and mixed coniferous and broadleaf and deciduous forest and woodland. Results are less contrasted for the correlation between the values of H_r and altitude. For all the vegetation biomes, the correlation value is lower than 0.4 except for the desert, where it is equal to 0.42. Higher correlation values were obtained when the correlation values were calculated between H_r values and the topography slopes. The highest correlation values ($r > 0.4$) were obtained for shrubs and bare ground, tundra and deserts.

5. Discussion

In this study, several assumptions were made and they may have an impact on the retrieved values of H_r. They are discussed in the following paragraphs. As for vegetation, it was assumed that the effective scattering albedo (ω) of all vegetation types is equal to zero and the tt_p parameters were set equal to zero. The latter hypothesis corresponds to an assumption of isotropic extinction effects by the canopy, which is often made in the literature. The chosen value of omega ($\omega = 0$) in

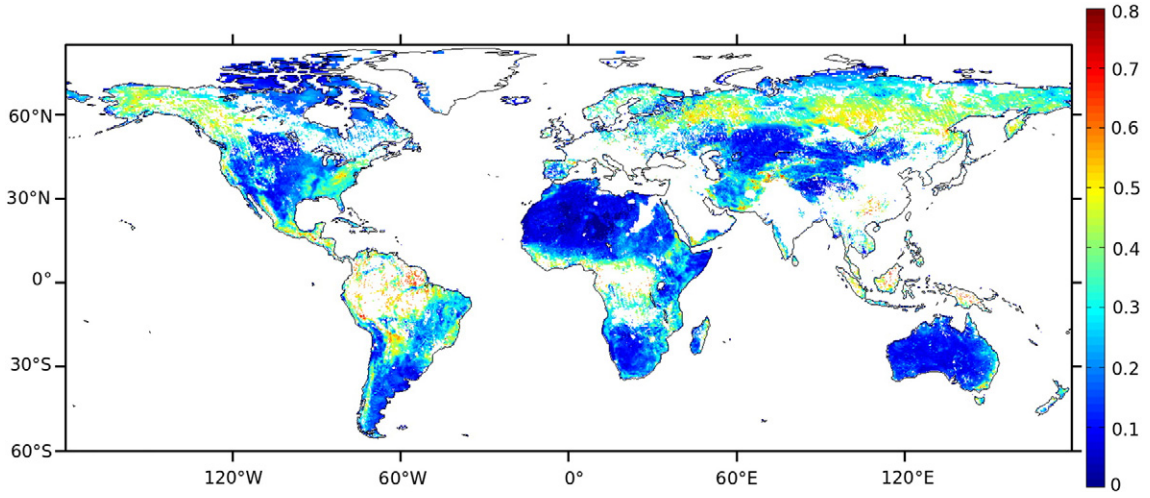

Fig. 11. Global roughness (H_r) map at L-band estimated from the SMOS data over 2011.

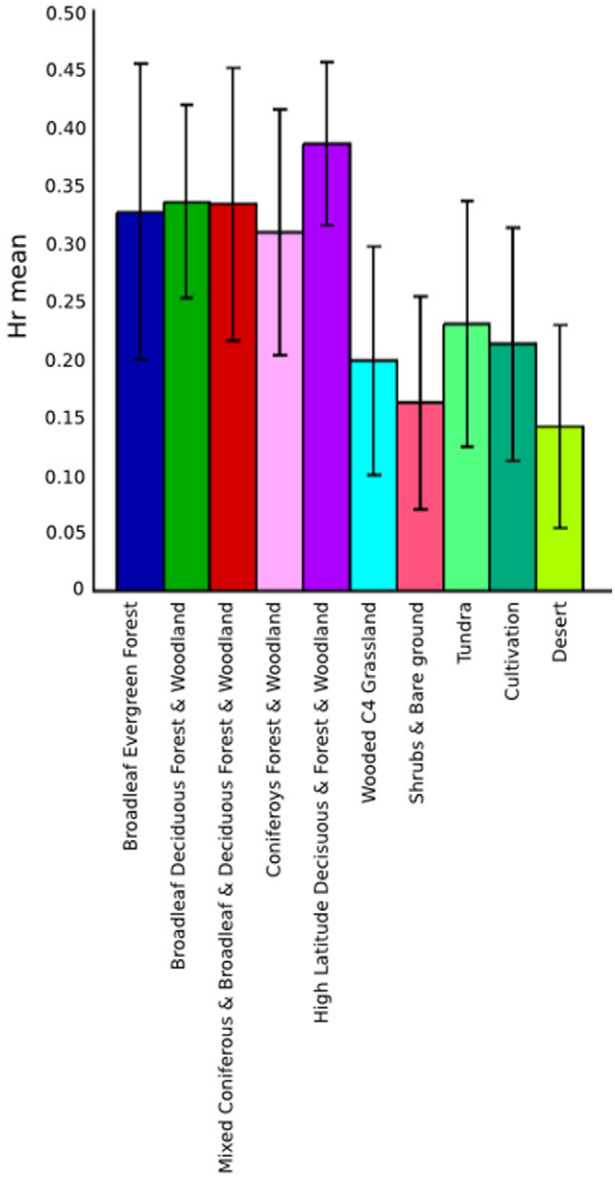

Fig. 12. Mean H_r values obtained at global scale with respect to the major vegetation biomes as defined in Dirmeyer et al. (2006).

this study may have too an impact on the retrieved values of H_r. However we expect that this impact is relatively small, as values of ω are generally found to be close to zero in the literature: ω values are close to zero for low vegetation types ($\omega \approx 0-0.03$), if we except some specific crop types as corn, and close to 0.06 for forests. Moreover, Konings et al. (2016) found that the impact of roughness was relatively low on the estimated value of ω (we expect the reverse is true). Presently, even if we expect this will be modified in the near future, the value of ω is set equal to zero over low vegetation and equal to 0.06 over forests in the operational SMOS algorithm. So the hypothesis made in this study is consistent with what is done in the SMOS algorithm, to the exception of forest canopies. Future works should attempt to improve the first results obtained in this study, by better accounting for vegetation scattering effects. This is a difficult task considering that the SMOS pixels generally include a variety of vegetation covers whose scattering properties may be very different and are not widely known to date.

As for soils, the Q_r and N_{rp} parameters were set equal, respectively, to 0 and −1 in this study. Using $N_{rp} = -1$ (i.e. combining vegetation and soil roughness effects in one single parameter) was recently found to be one of the best approaches in inversion studies (Fernandez-Moran et al., 2015; Parrens, Wigneron et al., 2014). The use of $Q_r = 0$ was generally made at L-band in the literature. However, strictly speaking, Q_r should not be equal to zero (Lawrence et al., 2014) especially in hilly terrain. However, the use of $Q_r = 0$, generally leads to very good results in inversion problems as the effects of Q_r can be partially accounted for by the value H_r (Lawrence et al., 2014). Moreover, presently, there is no clear method to calibrate Q_r and the assumption $Q_r = 0$, is made too in the operational SMOS algorithm.

The methodology presented in this study allowed us to decouple the effects of vegetation (τ_{nad}) and soil roughness (H_r). So, the optical depth (τ_{nad}) can be derived from the retrieved value of TR, by subtracting roughness effects (Eq. (6)), assuming, as done in this study, that these roughness effects are constant over the year. The mean value of τ_{nad} over the continental surfaces is shown in Fig. 14. This figure was derived from Fig. 5, by subtracting the roughness effects (shown in Fig. 11 using Eq. (6)). There is no reference map of vegetation optical depth at L-band that can be used to check whether the use of the roughness map (Fig. 11) allowed to us to produce more accurate and/or realistic maps of vegetation optical depth. However, at global scale, considering all the vegetation biomes, the spatial correlation between LAI and TR was equal to 0.68. By computing τ_{nad} from TR, the spatial correlation between τ_{nad} and LAI slightly increased and was equal to 0.70. This result is going in the right direction.

As for vegetation, another key assumption was made in this study as we assumed that the vegetation optical depth (τ_{nad}) is linearly related to LAI. However, Lawrence et al. (2014) found that τ_{nad} values generally peaked later than MODIS LAI values over crop zones of the USA, with an estimated time difference of about 19 days. This can be explained by the fact τ_{nad} accounts for the vegetation water content of the whole canopy, including fruits which have a late development, whereas LAI only accounts for leaf development. Note that this delayed peak in τ_{nad} (vs. LAI) cannot be generalized to all canopies as the reverse was found, for instance, by Fernandez-Moran et al. (2015) over vineyards. The assumption of a linear relationship between τ_{nad} and LAI was found by Wigneron et al. (2007) to be relatively correct during most of the vegetation growth over crops and we expect that the

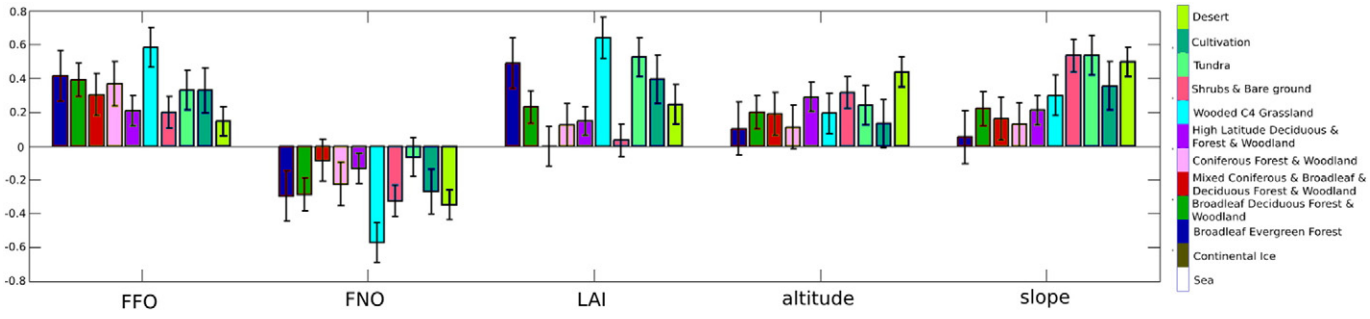

Fig. 13. Correlation (r) values between the values of H_r and FFO, FNO, LAI, altitude and topography slopes with respect to the major vegetation biomes as defined in Dirmeyer et al. (2006).

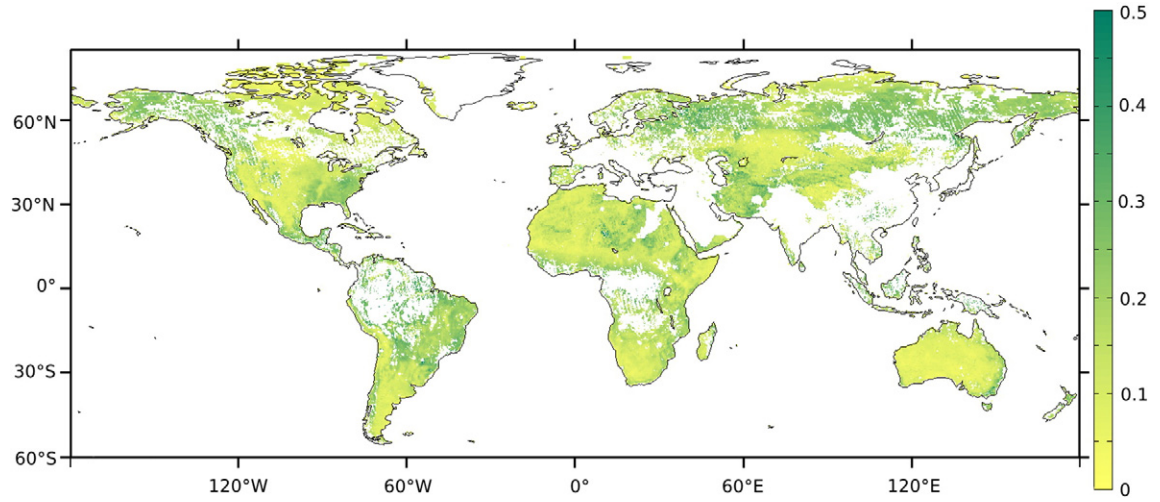

Fig. 14. Global vegetation optical depth (τ_{nad}) map obtained by computing τ_{nad} from the TR parameter (given in Fig. 5) using the global roughness map of H_r (given in Fig. 11).

computation of the intercept of this linear relationship shows little sensitivity to non-linear effects between τ_{nad} and LAI at the end of the vegetation growth.

6. Conclusion

A first attempt to map the surface effects as seen in the SMOS observations has been presented in this study. The general approach is relatively similar to the one developed by Wang et al. (2015) from observations of AMSR-E at C-band. In both studies (Wang's and the present one), the main general idea was to retrieve a combined vegetation roughness parameter (referred to as TR in this study) and then to decouple the effects of vegetation and roughness using information on the seasonal variations in vegetation from MODIS LAI observations.

However, there are several differences in the general methodology developed in this study. Firstly, we distinguished pixels corresponding to bare soil or sparsely vegetated surfaces (case 1) and vegetated pixels (case 2). Over pixels corresponding to case 1, the TR parameter accounted mainly for roughness effects (the vegetation optical thickness was assumed to be negligible) and the computation of H_r was direct ($H_r \sim 2 \times \mathrm{TR}$).

Secondly, over vegetated surfaces (case 2), we masked pixels where the sensitivity of the SMOS TB observations to the surface effects was found to be very low. These pixels represent almost 13% of the land surfaces. This step was performed to filter out pixels where the vegetation density was so high that the impact of the surface effects on the SMOS TB observations was almost negligible.

Thirdly, the retrievals of TR from the AMSRE and the SMOS TB data were not carried out in the same way. For the AMSR-E data, TR was found from an analytical formulation computed from mono-angular and dual-polarized TB observations but, in the present study, simultaneous 2-parameter retrievals of TR and SM were made from multi-angular and dual-polarized SMOS observations.

Moreover, the main approximations made in this study concerning vegetation effects, namely considering the effective scattering albedo as negligible and assuming the vegetation optical depth to be linearly related to LAI, are often made at L-band, while they are more questionable at C-band.

The H_r values found in this study at L-band are generally in agreement with the values found at local scale in the literature. Lowest values ($H_r \sim 0.14$–0.23) were obtained over shrubs and bare ground, cultivated land, wooded C4 grassland, tundra and desert (Fig. 12). This is in agreement with studies made over crop fields and low vegetation covers (Cano et al., 2010; Escorihuela et al., 2007; Lawrence et al., 2013; Mo et al., 1982; Saleh et al., 2007; Schlenz et al., 2012; Wang et al., 1982; Wigneron et al., 2001, 2007, 2011, 2012 and among others). For instance, the default value of H_r considered in the SMOS algorithm over low vegetation covers is 0.1. Higher values were obtained over forests ($H_r \sim 0.32$–0.39). This is also in agreement with the literature. For instance, the default value of H_r considered in the SMOS algorithm over forests is 0.3 (Ferrazzoli et al., 2002). It is likely that the higher values of the H_r parameter over forests can be related to the effects of litter, which are implicitly accounted for by the H_r parameter (Grant et al., 2007; Grant et al., 2008; Saleh et al., 2006). The high correlation computed between H_r and LAI over wooded C4 grassland could also be an indirect effect related to litter.

As confirmed in this study the H_r parameter computed is an effective parameter that accounts for roughness effects, litter and also topography. In particular, significant correlation values and correlation coefficients >0.4 were computed between the values of H_r and topography slopes over tundra, desert, shrubs and bare ground.

Future studies need to be carried out to evaluate how the soil roughness maps at L-band computed in this study could be useful to improve the soil moisture retrievals from the L-band SMOS and SMAP sensors. Recent studies have shown that the use of 2-parameter retrievals of SM and TR (combining vegetation and soil roughness effects) is very efficient to estimate SM from multi-angular observations (Parrens, Wigneron et al., 2014; Rodriguez-Fernandez et al., 2014). In that case, no a priori estimates of H_r are required in the inversion process of SM from the SMOS observations. Moreover, contrary to what is assumed here, it is not necessary to consider that the roughness parameter H_r is constant over time. Nevertheless, the values of H_r computed in this study can be useful to compute the vegetation optical depth τ_{nad} from the combined vegetation–roughness TR parameter. The interest of the maps of H_r plotted in this study also has to be evaluated for SM retrievals computed from SMAP observations. Presently, in the SMAP algorithm (ONeill, Chan, Njoku, Jackson, & Bindlish, 2012) the values of the H_r parameter are computed as a function of the main vegetation categories, but these tables were mainly established from TB observations made from tower-based or airborne sensors, which could not be representative of the large footprints of space-borne TB observations.

Acknowledgments

The authors would like to thank the TOSCA (Terre Ocean Surfaces Continentales et Atmosphere) CNES program for funding this research work and the two anonymous reviewers for their helpful comments.

References

Al Bitar, A., Mialon, A., Kerr, Y., Jacquette, E., Cabot, F., Richaume, P., Quesney, A., Tarrot, S., Parrens, M., Tomer, S., Molero, B., Pellarin, T., Al-Yaari, A., Wigneron, J., The SMOS level 3 daily soil moisture maps using multi-orbit retrieval algorithm. (in preparation).

Al-Yaari, A., Wigneron, J. P., Ducharne, A., Kerr, Y., De Rosnay, P., De Jeu, R., Govind, A., Al Bitar, A., Albergel, C., Munoz-Sabater, J., et al. (2014a). Global-scale evaluation of two satellite-based passive microwave soil moisture datasets (SMOS and AMSR-E) with respect to land data assimilation system estimates. *Remote Sensing of Environment*, *149*, 181–195.

Al-Yaari, A., Wigneron, J. P., Ducharne, A., Kerr, Y., Wagner, W., De Lannoy, G., Reichle, R., Al Bitar, A., Dorigo, W., Richaume, P., et al. (2014b). Global-scale comparison of passive (SMOS) and active (ASCAT) satellite based microwave soil moisture retrievals with soil moisture simulations (MERRA-Land). *Remote Sensing of Environment*, *152*, 614–626.

Armstrong, R., Brodzik, M., & Varani, A. (1997). The NSIDC ease-grid: Addressing the need for a common, flexible, mapping and gridding scheme. *Earth System Monitor*, *7*, 3.

Bindlish, R., Jackson, T. J., Wood, E., Gao, H., Starks, P., Bosch, D., & Lakshmi, V. (2003). Soil moisture estimates from TRMM microwave imager observations over the Southern United States. *Remote Sensing of Environment*, *85*, 507–515.

Cano, A., Saleh, K., Wigneron, J. P., Antolín, C., Balling, J. E., Kerr, Y. H., Kruszewski, A., Millán-Scheiding, C., Søbjærg, S. S., Skou, N., et al. (2010). The SMOS Mediterranean Ecosystem L-Band Characterisation Experiment (MELBEX-I) over natural shrubs. *Remote Sensing of Environment*, *114*, 844–853.

Dirmeyer, P. A., Gao, X., Zhao, M., Guo, Z., Oki, T., & Hanasaki, N. (2006). GSWP-2: Multimodel analysis and implications for our perception of the land surface. *Bulletin of the American Meteorological Society*, *87*, 1381–1397.

Entekhabi, D., Njoku, E., O'Neill, P., Kellogg, K., Crow, W., Edelstein, W., ... Van Zyl, J. (2010). The soil moisture active passive (SMAP) mission. *Proceedings of the IEEE*, *98*, 704–716. http://dx.doi.org/10.1109/JPROC.2010.2043918.

Escorihuela, M. J., Kerr, Y. H., de Rosnay, P., Wigneron, J. P., Calvet, J. C., & Lemaitre, F. (2007). A simple model of the bare soil microwave emission at L-band. *IEEE Transactions on Geoscience and Remote Sensing*, *45*, 1978–1987.

FAO, F. (1988). UNESCO soil map of the world, revised legend. *World Resources Report*, *60*, 138.

Fernandez-Moran, R., Wigneron, J. P., Lopez-Baeza, E., Al-Yaari, A., Coll-Pajaron, A., Mialon, A., Miernecki, M., Parrens, M., Salgado-Hernanz, P., Schwank, M., et al. (2015). Roughness and vegetation parameterizations at L-band for soil moisture retrievals over a vineyard field. *Remote Sensing of Environment*, *170*, 269–279.

Ferrazzoli, P., Guerriero, L., & Wigneron, J. P. (2002). Simulating L-band emission of forests in view of future satellite applications. *IEEE Transactions on Geoscience and Remote Sensing*, *40*, 2700–2708.

Grant, J., Wigneron, J. P., Van de Griend, A., Kruszewski, A., Søbjærg, S. S., & Skou, N. (2007). A field experiment on microwave forest radiometry: L-band signal behaviour for varying conditions of surface wetness. *Remote Sensing of Environment*, *109*, 10–19.

Grant, J. P., Saleh-Contell, K., Wigneron, J. P., Guglielmetti, M., Kerr, Y. H., Schwank, M., ... Van de Griend, A. A. (2008). Calibration of the L-MEB model over a coniferous and a deciduous forest. *IEEE Transactions on Geoscience and Remote Sensing*, *46*, 808–818.

Jackson, T., & Le Vine, D. E. (1996). Mapping surface soil moisture using an aircraft-based passive microwave instrument: Algorithm and example. *Journal of Hydrology*, *184*, 85–99.

Jackson, T., Schmugge, T., & O'Neill, P. (1984). Passive microwave remote sensing of soil moisture from an aircraft platform. *Remote Sensing of Environment*, *14*, 135–151.

Jackson, T. J. (1980). Profile soil moisture from space measurements. *Journal of the irrigation and drainage division. American Society of Civil Engineers*. (pp. 81–92).

Jackson, T. J. (1993). Measuring surface soil moisture using passive microwave remote sensing. *Hydrological Processes*, *7*, 139–152.

Jackson, T. J., Hsu, A. Y., & O'Neill, P. E. (2002). Surface soil moisture retrieval and mapping using high-frequency microwave satellite observations in the Southern Great Plains. *Journal of Hydrometeorology*, *3*, 688–699.

Jarvis, A., Reuter, H. I., Nelson, A., & Guevara, E. (2008). *Hole-filled SRTM for the globe version 4. Available from the CGIAR-CSI SRTM 90m database (http://srtm.csi.cgiar.org)*.

Kerr, Y., Waldteufel, P., Richaume, P., Wigneron, J., Ferrazzoli, P., & Gurney, R. (2010a). SMOS level 2 processor for soil moisture Algorithm Theoretical Based Document (ATBD), CESBIO, Toulouse. *Technical report. France, tech. rep. SO-TN-ESL-SM-GS-0001*.

Kerr, Y., Waldteufel, P., Richaume, P., Wigneron, J. P., Ferrazzoli, P., Mahmoodi, A., ... Delwart, S. (2012). The SMOS soil moisture retrieval algorithm. *IEEE Transactions on Geoscience and Remote Sensing*, *50*, 1384–1403. http://dx.doi.org/10.1109/TGRS.2012.2184548.

Kerr, Y., Waldteufel, P., Wigneron, J., Martinuzzi, J., Font, J., & Berger, M. (2001). Soil moisture retrieval from space: The soil moisture and ocean salinity (SMOS) mission. *IEEE Transactions on Geoscience and Remote Sensing*, *39*, 1729–1735.

Kerr, Y., Waldteufel, P., Wigneron, J. P., Delwart, S., Cabot, F., Boutin, J., ... Mecklenburg, S. (2010b). The SMOS mission: New tool for monitoring key elements ofthe global water cycle. *Proceedings of the IEEE*, *98*, 666–687. http://dx.doi.org/10.1109/JPROC.2010.2043032.

Kirdyashev, K., Chukhlantsev, A., & Shutko, A. (1979). The microwave emission of the earth in the presence of a vegetation canopy. *Radiotekhnika i Elektronika*, 256.

Konings, A. G., Piles, M., Rötzer, K., McColl, K. A., Chan, S. K., & Entekhabi, D. (2016). Vegetation optical depth and scattering albedo retrieval using time series of dual-polarized L-band radiometer observations. *Remote Sensing of Environment*, *172*, 178–189.

Kurum, M. (2013). Quantifying scattering albedo in microwave emission of vegetated terrain. *Remote Sensing of Environment*, *129*, 66–74.

Lawrence, H., Wigneron, J. P., Demontoux, F., Mialon, A., & Kerr, Y. (2013). Evaluating the semiempirical h–q model used to calculate the L-band emissivity of a rough bare soil. *IEEE Transactions on Geoscience and Remote Sensing*, *51*, 4075–4084. http://dx.doi.org/10.1109/TGRS.2012.2226995.

Lawrence, H., Wigneron, J. P., Richaume, P., Novello, N., Grant, J., Mialon, A., Al Bitar, A., Merlin, O., Guyon, D., Leroux, D., et al. (2014). Comparison between SMOS vegetation optical depth products and modis vegetation indices over crop zones of the usa. *Remote Sensing of Environment*, *140*, 396–406.

Merlin, O., Walker, J. P., Panciera, R., Escorihuela, M. J., & Jackson, T. J. (2009). Assessing the SMOS soil moisture retrieval parameters with high-resolution NAFE'06 data. *IEEE Geoscience and Remote Sensing Letters*, *6*, 635–639.

Mironov, V., Kerr, Y., Wigneron, J. P., Kosolapova, L., & Demontoux, F. (2013). Temperature- and texture-dependent dielectric model for moist soils at 1.4 GHz. *IEEE Geoscience and Remote Sensing Letters*, *10*, 419–423.

Mladenova, I., Jackson, T., Njoku, E., Bindlish, R., Chan, S., Cosh, M., Holmes, T., de Jeu, R., Jones, L., Kimball, J., et al. (2014). Remote monitoring of soil moisture using passive microwave-based techniques—Theoretical basis and overview of selected algorithms for AMSR-E. *Remote Sensing of Environment*, *144*, 197–213.

Mo, T., Choudhury, B., Schmugge, T., Wang, J., & Jackson, T. (1982). A model for microwave emission from vegetation-covered fields. *Journal of Geophysical Research: Oceans (1978–2012)*, *87*, 11229–11237.

MOD13A2, MCD15A2, U.R.O., Science (EROS) center, Sioux Falls, S.D. (2010a). *Modis, NASA land processes distributed active archive center (LP DAAC)*.

Montpetit, B., Royer, A., Wigneron, J. P., Chanzy, A., & Mialon, A. (2015). Evaluation of multi-frequency bare soil microwave reflectivity models. *Remote Sensing of Environment*, *162*, 186–195.

Njoku, E., Jackson, T., Lakshmi, V., Chan, T., & Nghiem, S. (2003). Soil moisture retrieval from AMSR-E. *IEEE Transactions on Geoscience and Remote Sensing*, *41*, 215–229.

Njoku, E. G., & Chan, S. K. (2006). Vegetation and surface roughness effects on AMSR-E land observations. *Remote Sensing of Environment*, *100*, 190–199.

Njoku, E. G., Wilson, W. J., Yueh, S. H., Dinardo, S. J., Li, F. K., Jackson, T. J., ... Bolten, J. (2002). Observations of soil moisture using a passive and active low-frequency microwave airborne sensor during SGP99. *IEEE Transactions on Geoscience and Remote Sensing*, *40*, 2659–2673.

Oliva, R., Daganzo, E., Kerr, Y. H., Mecklenburg, S., Nieto, S., Richaume, P., & Gruhier, C. (2012). SMOS radio frequency interference scenario: Status and actions taken to improve the rfi environment in the 1400–1427-MHz passive band. *IEEE Transactions on Geoscience and Remote Sensing*, *50*, 1427–1439.

ONeill, P., Chan, S., Njoku, E., Jackson, T., & Bindlish, R. (2012). *SMAP level 2 & 3 soil moisture (passive) algorithm theoretical basis document (ATBD). Initial release, version 1*.

Owe, M., de Jeu, R., & Walker, J. (2001). A methodology for surface soil moisture and vegetation optical depth retrieval using the microwave polarization difference index. *IEEE Transactions on Geoscience and Remote Sensing*, *39*, 1643–1654.

Panciera, R., Walker, J. P., & Merlin, O. (2009b). Improved understanding of soil surface roughness parameterization for L-band passive microwave soil moisture retrieval. *IEEE Geoscience and Remote Sensing Letters*, *6*, 625–629.

Panciera, R., Walker, J. P., Kalma, J. D., Kim, E. J., Saleh, K., & Wigneron, J. P. (2009a). Evaluation of the SMOS L-MEB passive microwave soil moisture retrieval algorithm. *Remote Sensing of Environment*, *113*, 435–444.

Panciera, R., Walker, J. P., Jackson, T. J., Gray, D., Tanase, M., Ryu, D., Monerris, A., Yardley, H., Rudiger, C., Wu, X., et al. (2014). The soil moisture active passive experiments (SMAPEX): Toward soil moisture retrieval from the smap mission. *IEEE Transactions on Geoscience and Remote Sensing*, *52*, 490–507.

Parrens, M., Mahfouf, J. F., Barbu, A., & Calvet, J. C. (2014a). Assimilation of surface soil moisture into a multilayer soil model: Design and evaluation at local scale. *Hydrology and Earth System Sciences*, *18*, 673–689.

Parrens, M., Wigneron, J. P., Richaume, P., Al Bitar, A., Mialon, A., Wang, S., ... Kerr, Y. (2016). *Considering combined or separated roughness and vegetation effects in soil moisture retrievals.* (In review on IEEE TGRS).

Parrens, M., Wigneron, J. P., Richaume, P., Kerr, Y., Wang, S., Alyaari, A., ... Grant, J. P. (2014b). Global maps of roughness parameters from L-band SMOS observations, in: Geoscience and Remote Sensing Symposium (IGARSS), 2014 IEEE International. *IEEE*, 4675–4678.

Peischl, S., Walker, J. P., Ryu, D., Kerr, Y. H., Panciera, R., & Rüdiger, C. (2012). Wheat canopy structure and surface roughness effects on multiangle observations at L-band. *IEEE Transactions on Geoscience and Remote Sensing*, *50*, 1498–1506.

Pellarin, T., Tran, T., Cohard, J. M., Galle, S., Laurent, J. P., Rosnay, P. d., & Vischel, T. (2009). Soil moisture mapping over West Africa with a 30-min temporal resolution using AMSR-E observations and a satellite-based rainfall product. *Hydrology and Earth System Sciences*, *13*, 1887–1896.

Rahmoune, R., Ferrazzoli, P., Singh, Y. K., Kerr, Y. H., Richaume, P., & Al Bitar, A. (2014). SMOS retrieval results over forests: Comparisons with independent measurements. *IEEE Journal of Selected Topics in Applied Earth Observations and Remote Sensing*, *7*, 3858–3866.

Rodriguez-Fernandez, N., Richaume, P., Aires, F., Prigent, C., Kerr, Y., Kolassa, J., ... Mahmoodi, A. (2014). Soil moisture retrieval from SMOS observations using neural networks, in: Geoscience and Remote Sensing Symposium (IGARSS), 2014 IEEE International. *IEEE*, 2431–2434.

Saleh, K., Kerr, Y. H., Richaume, P., Escorihuela, M., Panciera, R., Delwart, S., Boulet, G., Maisongrande, P., Walker, J., Wursteisen, P., et al. (2009). Soil moisture retrievals at L-band using a two-step inversion approach (CoSMOS/NAFE'05 experiment). *Remote Sensing of Environment*, *113*, 1304–1312.

Saleh, K., Wigneron, J., Calvet, J., Lopez-Baeza, E., Ferrazzoli, P., Berger, M., ... Miller, J. (2004). The eurostarrs airborne campaign in support of the SMOS mission: First results over land surfaces. *International Journal of Remote Sensing*, *25*, 177–194.

Saleh, K., Wigneron, J. P., de Rosnay, P., Calvet, J. C., & Kerr, Y. (2006b). Semi-empirical regressions at L-band applied to surface soil moisture retrievals over grass. *Remote Sensing of Environment*, *101*, 415–426.

Saleh, K., Wigneron, J. P., Waldteufel, P., De Rosnay, P., Schwank, M., Calvet, J. C., & Kerr, Y. (2007). Estimates of surface soil moisture under grass covers using L-band radiometry. *Remote Sensing of Environment*, *109*, 42–53.

Schlenz, F., Fallmann, J., Marzahn, P., Loew, A., & Mauser, W. (2012). Characterization of rape field microwave emission and implications to surface soil moisture retrievals. *Remote Sensing*, *4*, 247–270.

Schmugge, T. (1983). Remote sensing of soil moisture: Recent advances. *IEEE Transactions on Geoscience and Remote Sensing*, 336–344.

Schmugge, T., Jackson, T., Kustas, W., & Wang, J. (1992). Passive microwave remote sensing of soil moisture: Results from HAPEX, FIFE and MONSOON 90. *ISPRS Journal of Photogrammetry and Remote Sensing*, *47*, 127–143.

Skou, N., Misra, S., Balling, J. E., Kristensen, S. S., & Sobjaerg, S. S. (2010). L-band RFI as experienced during airborne campaigns in preparation for SMOS. *IEEE Transactions on Geoscience and Remote Sensing*, *48*, 1398–1407.

Ulaby, F. T. (1982). *Microwave remote sensing: Active and passive, radar remote sensing and surface scattering and emission theory. vol. 2*, Addison-Wesley: Reading, Mass.

Van de Griend, A., & Owe, M. (1994). Microwave vegetation optical depth and inverse modelling of soil emissivity using Nimbus/SMMR satellite observations. *Meteorology and Atmospheric Physics*, *54*, 225–239.

Wagner, W., Lemoine, G., & Rott, H. (1999). A method for estimating soil moisture from ers scatterometer and soil data. *Remote Sensing of Environment*, *70*, 191–207.

Wang, J., & Choudhury, B. (1981). Remote sensing of soil moisture content, over bare field at 1.4 GHz frequency. *Journal of Geophysical Research: Oceans (1978–2012)*, *86*, 5277–5282.

Wang, J. R., McMurtrey, J. E., Engman, E. T., Jackson, T. J., Schmugge, T. J., Gould, W. I., ... Glazar, W. S. (1982). Radiometric measurements over bare and vegetated fields at 1.4-GHz and 5-GHz frequencies. *Remote Sensing of Environment*, *12*, 295–311.

Wang, J. R., O'Neill, P. E., Jackson, T. J., & Engman, E. T. (1983). Multifrequency measurements of the effects of soil moisture, soil texture, and surface roughness. *IEEE Transactions on Geoscience and Remote Sensing*, 44–51.

Wang, S., Wigneron, J. P., Jiang, L. M., Parrens, M., Yu, X. Y., Al-Yaari, A., ... Kerr, Y. (2015). Global-scale evaluation of roughness effects on C-band AMSR-E observations. *Remote Sensing*, *7*, 5734–5757.

Wegmuller, U., & Matzler, C. (1999). Rough bare soil reflectivity model. *IEEE Transactions on Geoscience and Remote Sensing*, *37*, 1391–1395.

Wigneron, J. P., Chanzy, A., Calvet, J. C., & Bruguier, N. (1995). A simple algorithm to retrieve soil moisture and vegetation biomass using passive microwave measurements over crop fields. *Remote Sensing of Environment*, *51*, 331–341.

Wigneron, J. P., Chanzy, A., Kerr, Y., Lawrence, H., Shi, J., Escorihuela, M. J., ... Saleh-Contell, K. (2011). Evaluating an improved parameterization of the soil emission in L-MEB. *IEEE Transactions on Geoscience and Remote Sensing*, *49*, 1177–1189. http://dx.doi.org/10.1109/TGRS.2010.2075935.

Wigneron, J. P., Kerr, Y., Waldteufel, P., Saleh, K., Escorihuela, M. J., Richaume, P., ... Schwank, M. (2007). L-band microwave emission of the biosphere (L-MEB) model: Description and calibration against experimental data sets over crop fields. *Remote Sensing of Environment*, *107*, 639–655. http://dx.doi.org/10.1016/j.rse.2006.10.014.

Wigneron, J. P., Laguerre, L., & Kerr, Y. H. (2001). A simple parameterization of the L-band microwave emission from rough agricultural soils. *IEEE Transactions on Geoscience and Remote Sensing*, *39*, 1697–1707.

Wigneron, J. P., Schwank, M., Baeza, E. L., Kerr, Y., Novello, N., Millan, C., Moisy, C., Richaume, P., Mialon, A., Al Bitar, A., et al. (2012). First evaluation of the simultaneous SMOS and ELBARA-II observations in the Mediterranean region. *Remote Sensing of Environment*, *124*, 26–37.